ABSORPTION

1. Introduction

Absorption, or gas absorption, is a unit operation used in the chemical industry and increasingly in environmental applications to separate gases by washing or scrubbing a gas mixture with a suitable liquid. One or more of the constituents of the gas mixture dissolves or is absorbed in the liquid and can thus be removed from the mixture. In some systems, this gaseous constituent forms a physical solution with the liquid or the solvent. In other cases, it undergoes a chemical reaction with one or more components of the liquid.

The purpose of such scrubbing operations may be any of the following: gas purification (eg, removal of air pollutants from exhaust gases or contaminants from gases that will be further processed), product recovery, or production of solutions of gases for various purposes. Several examples of applied absorption processes are shown in Table 1.

Gas absorption is usually carried out in vertical countercurrent columns as shown in Figure 1. The solvent is fed at the top of the absorber, whereas the gas mixture enters from the bottom. The absorbed substance is washed out by the solvent and leaves the absorber at the bottom as a liquid solution. The solvent is often recovered in a subsequent stripping or desorption operation. This second

Table 1. **Typical Commercial Gas Absorption Processes**

Treated gas	Absorbed gas, solute	Solvent	Function
coke oven gas	ammonia	water	by-product recovery
coke oven gas	benzene and toluene	straw oil	by-product recovery
reactor gases in manufacture of formaldehyde from methanol	formaldehyde	water	product recovery
drying gases in cellulose acetate fiber production	acetone	water	solvent recovery
natural and refinery gases	hydrogen sulfide	amine solutions	pollutant removal
flue gases	sulfur dioxide	water	pollutant removal
	carbon dioxide	amine solutions	by-product recovery
wet well gas	propane and butane	kerosene	gas separation
wet well gas	water	triethyleneglycol	gas drying
ammonia synthesis gas	carbon monoxide	ammoniacal cuprous chloride solution	contaminant removal
roast gases	sulfur dioxide	water	production of calcium sulfite solution for pulping

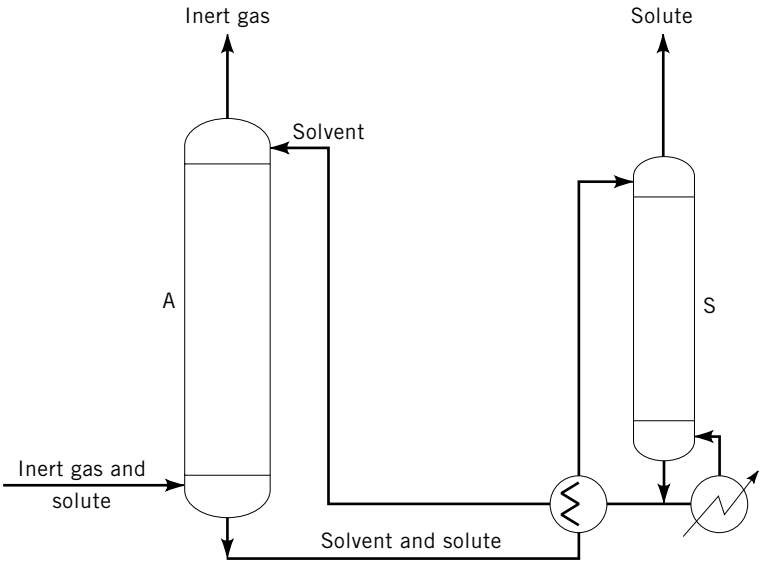

Fig. 1. Absorption column arrangement with a gas absorber A and a stripper S to recover solvent.

step is essentially the reverse of absorption and involves countercurrent contacting of the liquid loaded with solute using an inert gas or water vapor. Desorption is frequently carried out at higher temperatures and/or at lower pressure than the absorption step. The absorber may be a packed column, plate tower, or simple spray column, or a bubble column. The packed column is a shell either filled with randomly packed elements or having a regular solid structure designed to disperse the liquid and bring it and the rising gas into close contact. Dumped-type packing elements come in a great variety of shapes (Fig. 2**a**–**f**) and construction materials. These elements are intended to create a large internal surface but a small pressure drop. Structured, or arranged packings may be made of corrugated metal or plastic sheets providing a large number of regularly arranged channels (Fig. 2**g**), but a variety of other geometries exists. In plate towers, liquid flows from plate to plate in cascade fashion and gases bubble through the flowing liquid at each plate through a multitude of dispersers (eg, holes in a sieve tray, slits in a bubble-cap tray) or through a cascade of liquid as in a shower deck tray (see DISTILLATION).

The advantages of packed columns include simple and, as long as the tower diameter is not too large, usually relatively cheaper construction. These columns are preferred for corrosive gases because packing, but not plates, can be made from ceramic or plastic materials. Packed columns are also used in vacuum applications because the pressure drop, especially for regularly structured packings, is usually less than through plate columns. Tray absorbers are used in applications where tall columns are required, because tall, random-type packed towers are more prone to channeling and maldistribution of the liquid and gas streams. The sensitivity of packed columns to maldistribution is especially high in applications where the density difference between gas and liquid is small and the

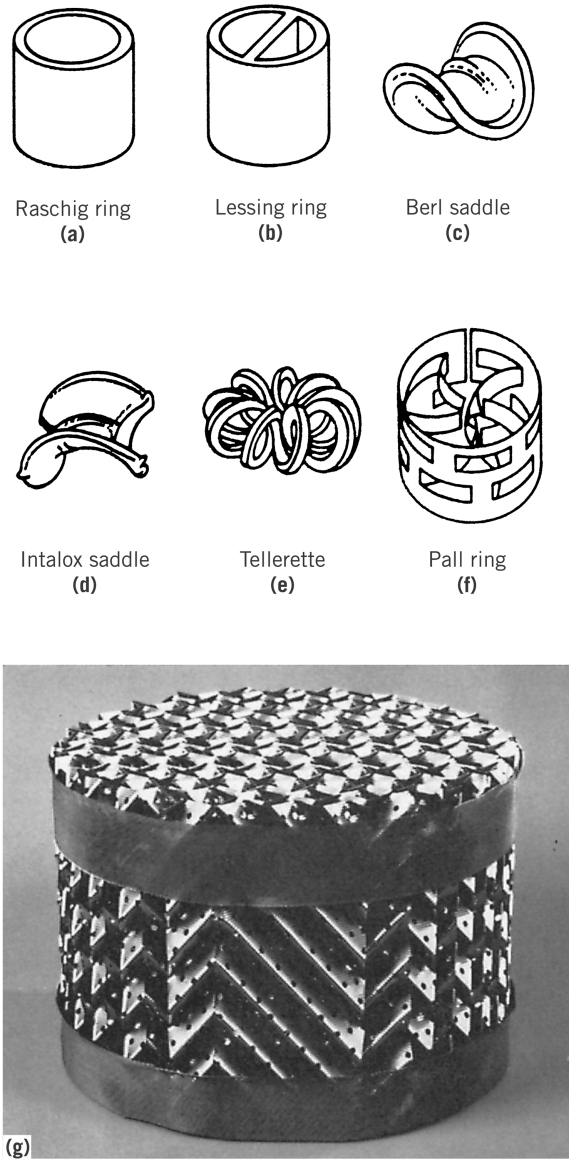

Fig. 2. Packing materials for packed columns. (**a**–**f**) Typical packing elements generally used for random packing; (**g**) example of structured packing. (**g**) Courtesy of Sulzer Bros. S.A. Winterthur, Switzerland.

interfacial tension between the liquid and the gas or vapor is lower than about 0.01 N m^{-1}. However, packings tend to have significantly higher capacity than trays for a given separation duty. This increased capacity makes them useful in revamping applications. On the other hand, plate towers can be more easily cleaned. Plates are also preferred in applications having large heat effects since cooling coils are more easily installed in plate towers and liquid can be

withdrawn more easily from plates than from packings for external cooling. Bubble trays can also be designed for large liquid holdup.

The fundamental physical principles underlying the process of gas absorption are the solubility of the absorbed gas and the rate of mass transfer. Information on both must be available when sizing equipment for a given application. Additionally, in the very frequent case of the design of countercurrent columns, it is also necessary to have information on the hydraulic capacity (eg, entrainment, loading, flooding) of the equipment. In addition to the fundamental design concepts based on solubility and mass transfer, many other practical details have to be considered during actual plant design and construction which may affect the performance of the absorber significantly. These details have been described in reviews (1) and in some of the more comprehensive treatments of gas absorption and absorbers (2–5) (see also DISTILLATION; HEAT EXCHANGE TECHNOLOGY).

2. Gas Solubility

At equilibrium, a component of a gas in contact with a liquid has identical fugacities in both the gas and liquid phase. For ideal solutions Raoult's law applies:

$$y_A = \frac{P_s}{P} x_A \tag{1}$$

where y_A is the mole fraction of A in the gas phase, P is the total pressure, P_s is the vapor pressure of pure A, and x_A is the mole fraction of A in the liquid. For moderately soluble gases with relatively little interaction between the gas and liquid molecules Henry's law is often applicable:

$$y_A = \frac{H}{P} x_A \tag{2}$$

where H is Henry's constant. Usually H is dependent upon temperature, but relatively independent of pressure at moderate levels. In solutions containing inorganic salts, H is also a function of the ionic strength. Henry's constants are tabulated for many of the common gases in water (6).

A more general way of expressing solubilities is through the vapor–liquid equilibrium constant m defined by

$$y_A = m x_A \tag{3}$$

The value of m, also known as equilibrium K value, is widely employed to represent hydrocarbon vapor–liquid equilibria in absorption and distillation calculations. When equation 1 or 2 is applicable at constant pressure and temperature (equivalent to constant m in eq. 3) a plot of y vs x for a given solute is linear from the origin. In other cases, the y–x plot may be approximated by a linear relationship over limited regions. Generally, for nonideal solutions or for nonisothermal conditions, y is a curving function of x and must be determined from experimental data or more rigorous theoretical relationships. In a y–x plot,

when applied to absorber design this function is commonly called the equilibrium line.

Obtaining reliable data on gas solubility for gas absorber design, in the form of Henry constats, m values or equations for the equilibrium line represents a major issue. Gas solubility has been treated extensively (7). Methods for the prediction of phase equilibria and actual solubility data have been given (8,9) and correlations of the equilibrium K values of hydrocarbons have been developed and compiled (10). Several good sources for experimental information on gas and vapor liquid equilibrium data of nonideal systems are also available (6,11–13). Several of these sources contain not only experimental data but also include models for correlating experimental data and for gas solubility prediction are based on equilibrium phase thermodynamics, involving equation of state and fugacities or Gibbs excess functions.

In addition to these phenomenological approaches, there exists a novel route based on statistical mechanics for the prediction of gas–liquid equilibrium based on a molecular description of gas and liquid. The field of molecular simulation (14–16) has advanced sufficiently in recent years so as to allow the computation of thermophysical data and multiphase equilibrium behavior. The key idea of such methods is to describe two or more phases in thermodynamic equilibrium by an atomistically detailed collection of interacting molecules. These simulation boxes contain a relatively small number of molecules (typically between a hundred and a million), which are endowed with proper geometry and interaction potentials (also known as the force field). A large number of individual configurations of these molecules is generated using methods such as molecular dynamics (MD) or Monte Carlo (MC). Macroscopic properties (eg, PvT) are obtained by averaging over the set of individual configurations. Depending on the constraints under which the MD or MC calculation is performed, different statistical mechanical ensembles can be generated. For equilibrium calculations, sophisticated techniques based on the so-called Gibbs ensemble (17) have been developed.

In a typical gas–liquid or vapor–liquid equilibrium simulation, two computational boxes, one representing the gas or vapor, the other representing the liquid, are "brought into equilibrium" by performing a series of MC moves, one of which is a particle exchange move. Although the compositions of the boxes fluctuate along the simulation due to particle interchanges, they do so about well-defined average values. In many cases, these average compositions closely match the values one would obtain in an equilibrium cell in a laboratory. A series of such calculations allows one to construct the full equilibrium line as required for absorber design. This procedure bypasses the need to use an equation of state for gas nonideality and an activity model for the liquid phase. The entire physicochemical complexity of the system is treated at the molecular level and is entirely represented by the geometry and the interaction potentials.

Such molecular techniques allow the prediction of thermophysical properties and phase equilibria under conditions that cannot be achieved easily in practice (eg, very high pressure, highly toxic or carcinogenic substances), or for compounds that have not been synthesized yet. Although they do not replace either traditional phase equilibrium calculations or experimental work, molecular simulations are a useful complement to both. They are particularly valuable

in the screening stages of new solvents for absorption. A molecular simulation can frequently help assess the suitability of a new compound or a new mixture of compounds for a given absorption application. They are also useful for new families of solvents or for mixtures of solvents that are not amenable to a group contribution approach, either because they contain a group that has not been tabulated yet or because there are strong interactions between groups that cannot be properly predicted by standard contribution mixing rules.

As an illustrative example a typical phase equilibrium calculation using molecular modeling techniques will be described in some detail. We will consider a binary system composed of a short-chain, linear hydrocarbon of length N_s as the solute (eg, ethane) and a long-chain linear hydrocarbon of length N_l as the solvent. We will consider two particular cases: $N_s = 2$, $N_l = 7$ and $N_s = 5$, $N_l = 150$. In the first case, we will be dealing with the phase equilibrium behavior of the system ethane–*n*-heptane and therefore with the solubility of ethane in *n*-heptane. The second system will demonstrate how the same approach can automatically be extended to the calculation of the solubility of low molecular weight compounds (pentane in this case) in molten polymers or high molecular weight solvents.

In standard molecular modeling, alkane molecules are considered classical mechanical systems in which atoms or atom groups, also called united atoms, are represented by interaction sites (see Fig. 3). Along a molecule, all pairs of sites i and j separated by more than three bonds along the chain and all intermolecular sites interact, in one of the simplest cases, via the Lennard–Jones pair potential:

$$V_{ij}^{\mathrm{LJ}}(r) = 4\epsilon_{ij}\left[\left(\frac{\sigma_{ij}}{r_{ij}}\right)^{12} - \left(\frac{\sigma_{ij}}{r_{ij}}\right)^{6}\right]$$

with r_{ij} being the scalar minimum-image distance between sites i and j and ε_{ij} and σ_{ij} being pair-specific interaction constants. In the case of polar molecules,

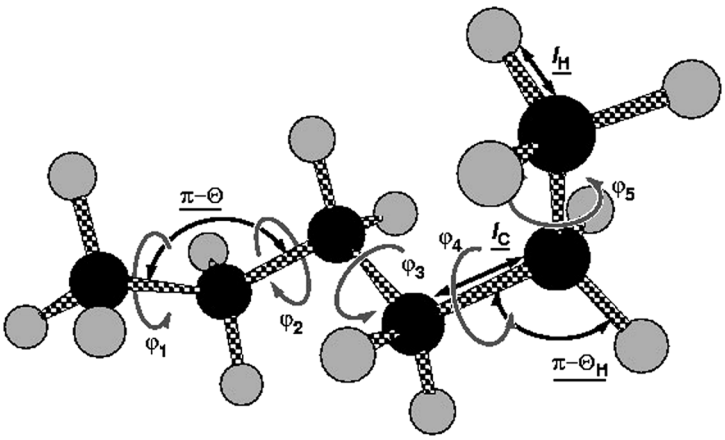

Fig. 3. Chain geometry and internal degrees of freedom of a linear alkane molecule. External degrees of freedom include translation and rotation as a rigid object.

additional electrostatic terms are added, using partial charges associated with interaction sites.

Besides the site–site interaction potential, additional (in the simplest case, harmonic) potentials are associated with bond stretching (18)

$$V_{\text{stretching}}(l) = \frac{1}{2}\ K_l(l - l_0)^2$$

where l is the bond length and l_0 the equilibrium bond length. Similarly, bond angle bending is endowed with a potential of the form:

$$V_{\text{bending}}(\theta) = \frac{1}{2}\ K_\theta(\theta - \theta_0)^2$$

where θ is the bond angle and θ is the equilibrium bond angle (19). Lastly, associated with each dihedral angle ϕ is also a torsional potential of the form (20):

$$V_{\text{torsion}}(\phi) = c_0 + c_1\ \cos(\phi) + c_2\ \cos(\phi)^2 + c_3\ \cos(\phi)^3 + c_4\cos(\phi)^4 + c_5\ \cos(\phi)^5$$

where ϕ is a specific torsion angle along the hydrocarbon chain backbone.

Several other terms (contributions) to the energy of a molecular system have been proposed. They represent higher order corrections and cross terms which couple, eg, bond stretching and bending, or account for out-of-plane deviations in planar molecules. In commercial molecular modeling software, the specific functional form of the interaction terms and the set of all parameters appearing in them is known as the "force field" and can contain several thousand parameters. For solubility calculations it is seldom necessary to consider the full set of interaction terms and those presented above are sufficient in many cases.

In order to evaluate each of the previous contributions to the energy of the system, the coordinates of all interaction sites of all molecules present in the system must also be computed. These are determined as a function of the external and internal degrees of freedom. External degrees of freedom are typically the absolute position of one of the sites of each molecule plus the absolute orientation in space of one bond of each molecule, expressed by means of Euler angles or by quaternions, with respect to a fixed laboratory frame of reference. Internal degrees of freedom are usually bond lengths, bond angles and torsional angles.

Once the absolute position and orientation of a reference site and a reference bond of each molecule and the internal degrees of freedom are known, it is possible to determine all site positions for all sites in all molecules using, e.g. the Eyring transfer matrix technique (20). In a last step, in order to eliminate edge effects which would mask the true behavior of the system, periodic boundary conditions, as originally introduced by Born (21) are applied to all site coordinates. Periodic boundary conditions are a necessity, since available computational power limits the characteristic size of systems that can be simulated to a few nanometers at the most.

Once the geometry of all chemical species and the force field describing their interactions are defined, the calculation of phase equilibrium is performed in the Gibbs ensemble, which was succinctly described above. The Gibbs

ensemble is a combination of the canonical (*NVT*), the isobaric–isothermal (*NPT*), and the grand-canonical ($N\mu T$) ensembles. In a molecular modeling Monte Carlo (MC) calculation, moves are performed sequentially in order to generate a Markov chain of system microstates. Macroscopic properties are obtained by simple averaging the corresponding properties for each of the microstates. In a Gibbs ensemble calculation, three types of MC are performed:

- *NVT* moves, in which molecular conformations in each of the simulation boxes are modified by one or more types of moves such as simple displacements, pivots, reptation, Continuous Configurational Bias, End Bridging, etc. (22).
- *NPT* moves, in which the volume of both boxes is changed in such a way that the total volume remains constant, ie, if one of the boxes is expanded by a given amount, the other is shrunk by the same amount.
- $N\mu T$ moves, in which particles are exchanged between boxes, ie, solute and solvent molecules can be transferred from one box to the other.

Each of these different types of moves is accepted or rejected with a certain probability. This probability depends directly (and strongly) on the change in the energy in the system induced by the move but also on the changes in volume and particle number. For example, the probability for a particle exchange ($N\mu T$ move) between boxes, denoted by I and II, to be accepted is given by:

$$min\ \left[1, \exp\left(\frac{1}{kT}\ \left[\Delta U^I + \Delta U^{II} + kT\ \ln\left[\frac{V^{II}(N^I+1)}{V^I N^{II}}\right]\right]\right)\right]$$

where ΔU is the change in the total energy (nonbonded intermolecular and intramolecular, bond stretching, bond bending and torsional) of a box (the superindex labels the box), V is the box volume, and N is the number of particles in the box. Analogous acceptance criteria are used for the other types of move. These criteria are defined so as to fulfill macroscopic equality of temperature, pressure and chemical potential between the boxes, i.e. thermodynamic phase equilibrium.

In a typical phase equilibrium calculation, a large number of MC steps of the three types described above are performed and system microstates (coordinates of atoms) are stored periodically together with properties of each of the simulation boxes, such as a density, potential energy, molar fraction of each component, etc. After a sufficiently large number of such MC steps have been performed, estimates of macroscopic properties, for example density, of each phase is obtained as the average of the densities of all the microstates generated in the MC run. Similarly, the composition of each phase is determined as the average of the compositions of each phase, which are trivially determined from the number of molecules of each species in each box for every microstate. Thus, a Gibbs ensemble calculation produces a pair of thermodynamically equilibrated phases, ie, a pair of points on the phase diagram of the two-component system (extensions to multicomponent systems are straightforward). A series of such calculations yields an equilibrium envelope describing the phase equilibria and therefore the mutual solubility of the two phases. In absorption calculations, the branch of the equilibrium envelope describing the solubility of the light

species in the heavy one is the most interesting one, although the other branch is of course useful, eg, in order to determine solvent losses.

A common feature of all molecular modeling techniques is that system nonidealities, high concentration effects, etc, are incorporated automatically and in a natural way in the calculation. In classical, equation of state (EOS)-based methods, saturation pressures, fugacities, activities and high-pressure correction factors enter the calculation separately. In molecular modeling, the full physicochemical complexity enters via the geometry and forcefield and needs never be split in separate contributions like fugacity, activity coefficients, etc.

The Gibbs ensemble calculation, provided the molecular description and the MC algorithms are correct, directly yields two phases in equilibrium. For this reason it is especially attractive for highly non-ideal systems, high-pressure systems or both. Molecular modeling is however not devoid of adjustable parameters: the values of the constants describing nonbonded interaction and bonded potentials (the force field parameters) are de facto adjustable parameters associated with specific atom types, just like parameters are associated with whole molecules, atom groups or single atoms in activity coefficient models and group contribution techniques. It is, however, generally felt that the force field parameters are better transferable among widely varying chemical families. This is especially justified in cases in which the parameters of the force field stem from a quantum chemical calculation.

Figure 4 shows the vapor–liquid equilibrium envelope (experimental data from (23)) for the system ethane–*n*-heptane at 58.71 mol% ethane. Symbols

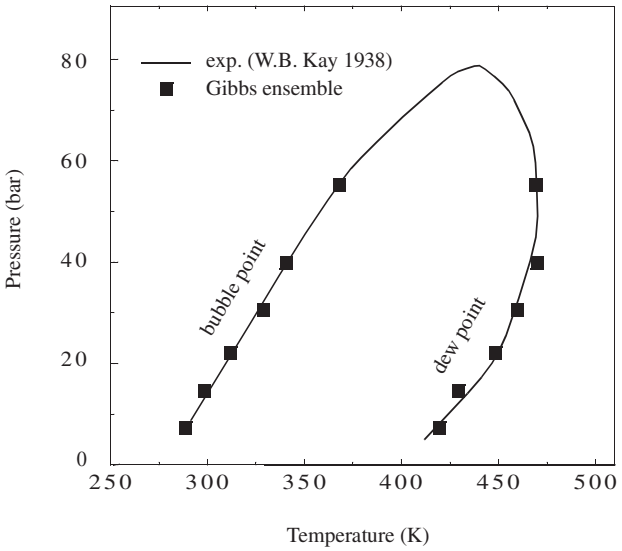

Fig. 4. Comparison of experimental (continuous line) and Gibbs ensemble simulation results for the vapor–liquid equilibrium of the ethane/heptane system. This diagram was constructed from a series of Gibbs ensemble simulations aimed at locating the dew and bubble points of a mixture of given composition. The construction of his diagram requires a great deal more effort than a typical solubility calculation (ie, given pressure and temperature, unknown compositions of the phases) which involves a single Gibbs ensemble simulation.

denote the results of a series of MC calculations in the Gibbs ensemble for the same system ($N_s = 2$, $N_l = 7$).

For this system, the agreement between experimental measurements and Gibbs ensemble calculations is remarkably good. In this relatively simple case, however, an advanced EOS approach (24–26) would also work very well and probably surpass the molecular modeling results in accuracy. The advantages of molecular modeling are more obvious when dealing with highly nonideal, high pressure systems or with new compounds or complex mixtures for which no experimental data are available and group contribution methods are known to be unreliable.

One such situation is the calculation of the solubility of short-chain alkanes (pentane) in molten linear polyethylene, $N_s = 5$, $N_l = 150$. Although hydrocarbon chains with $N_l = 150$ carbon atoms in the backbone are, strictly speaking, not yet polymers but high oligomers, they are however a reasonably good representation of a simple linear polymer such as polyethylene (PE).

Figure 5 shows experimental values of the solubility of pentane in polyethylene at infinite dilution (Henry's constant) and a series of Gibbs ensemble results at increasingly high pressures (27,28). At low pressures the results of Gibbs-ensemble and infinite-dilution data are consistent. At moderate pressures, deviations from Henry's law become significant. Finally, at pressures >20 bar, the polymer reaches the saturation limit and the solubility of pentane does not grow as rapidly as predicted by the linear extrapolation implicit in Henry's law.

These two examples of molecular modeling-based calculation of solubility illustrate the range of applicability of such atomistic techniques to phase equilibrium. However, they are also applicable to the determination of transport

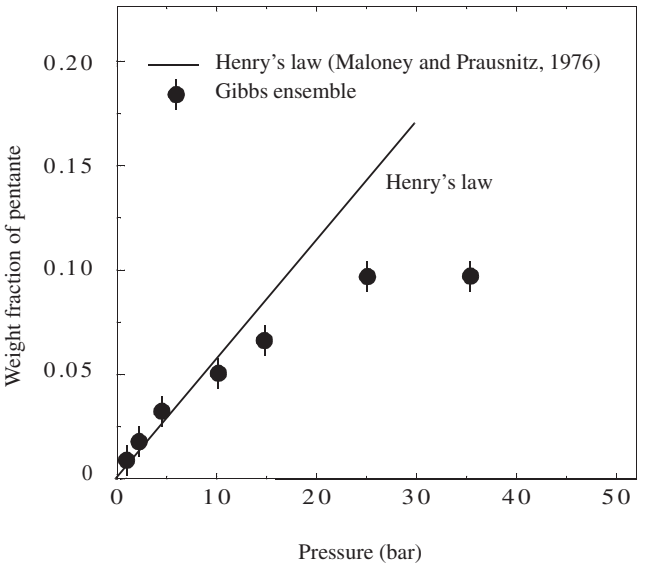

Fig. 5. Comparison of experimental (straight line) and Gibbs ensemble simulation results for the solubility of pentane in polyethylene. As the solvent saturates with pentane at high pressures, solubility deviates from the linearity predicted by Henry's law.

properties. An interesting application of these techniques to absorption technology is in the calculation of molecular diffusivities by means of molecular dynamics (MD). Its detailed treatment is out of the scope of this article but the interested reader can find an extensive description in (14).

It must, however, be kept in mind that the great power and generality of molecular modeling is achieved at the expense of massive computational effort: the calculation of a single pair of data points in the ethane–*n*-heptane diagram presented above requires several hours of calculation on state-of-the-art hardware, whereas the same calculation can be performed following the standard EOS approach in a few milliseconds. Molecular modeling techniques should therefore be applied judiciously and be reserved for those cases in which conventional methods fail or where their reliability is questionable.

The possibility to test a large number of alternative formulations of mixtures of solvents or pure compounds for their suitability for a particular application has made it possible to actually "design" solvents on a purely computational basis. Needless to say, such "designed" compounds or formulations must be subsequently tested in a laboratory or in a pilot plant in order to verify their effectiveness. Tests have shown molecular calculations to be remarkably successful at predicting solvent performance in many cases (29–31).

User-friendly molecular simulation packages already exist that allow phase equilibria calculations to be set up and performed relatively rapidly and with a modicum of effort on the part of the user. Nevertheless, it must be emphasized that molecular modeling approaches to solubility calculation will remain many orders of magnitude slower than EOS methods for the foreseeable future. It is therefore very doubtful that they will ever be used directly in single column let alone flowsheet simulators, where solubility calculations must be performed a very large number of times. A single MC calculation of gas solubility in a binary system takes nowadays significantly longer than the calculation of an entire plant flowsheet of average complexity. Increases in computer peformance will reduce the time required for MC or MD calculations, but so will they reduce the time required for EOS calculation, so that the ratio of computational effort will very likely remain close to its present value. For this reason, the greatest utility of molecular modeling methods is in generating a database of "computer-experimental" solubility values to which a suitable EOS can be fitted. It is this EOS that finds use in column and flowsheet simulators.

In spite of this computational disadvantage, the molecular computational approach to phase equilibrium and solvent design will probably see increased use in coming years.

3. Mass Transfer Concepts

3.1. Mass Transfer Coefficients and Driving Forces. In order to determine the size of the equipment necessary to absorb a given amount of solvent per unit time, one must know not only the equilibrium solubility of the solute in the solvent, but also the rate at which the equilibrium is established; ie, the rate at which the solute is transferred from the gas to the liquid phase must be determined. One of the first theoretical models describing the process

proposed an essentially stable gas-liquid interface (32). Large fluid motions are presumed to exist at a certain distance from this interface distributing all material rapidly and equally in the bulk of the fluid so that no concentration gradients are developed. Closer to this interface, however, the fluid motions are impaired and the slow process of molecular diffusion becomes more important as a mechanism of mass transfer. The rate-governing step in gas absorption is therefore the transfer of solute through two thin gas and liquid films adjacent to the phase interface. Transfer of materials through the interface itself is normally presumed to take place instantaneously so that equilibrium exists between these two films precisely at the interface. Although this assumption has been confirmed in experiments utilizing many systems and different types of phase interface (17,33–36), interfacial resistances can develop in some situations (37–42).

The resulting concentration profile is shown in Figure 6. With the passage of time in a nonflowing closed system, the profiles would become straight horizontal lines as the bulk gas and bulk liquid reached equilibrium. In a flowing system, Figure 6 represents conditions at some countercurrent flow point, eg, at a certain height in an absorption tower where, as gas and liquid pass each other, the bulk materials do not have sufficient contact time to attain equilibrium. Solute is continuously transferred from the gas to the liquid and concentration gradients develop when this transfer proceeds at only a finite rate.

The experimentally observed rates of mass transfer are often proportional to the displacement from equilibrium and the rate equations for the gas and liquid films are

$$N_A = k_G(p_A - p_{Ai}) = k_G P(y_A - y_{Ai}) \tag{4}$$

$$N_A = k_L(c_{Ai} - c_A) = k_L \bar{\rho}(x_{Ai} - x_A) \tag{5}$$

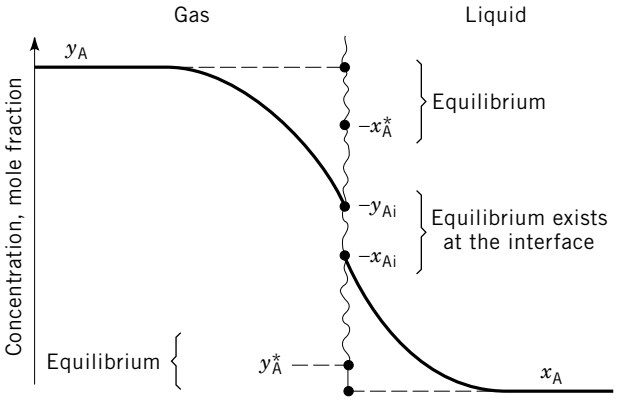

Fig. 6. The two-film concept: y_A and x_A are the concentrations in the bulk of the phases; y_{Ai} and x_{Ai} are the actual interfacial concentrations at equilibrium; y^*_A and x^*_A are the hypothetical equilibrium concentrations which would be in equilibrium with the bulk concentration of the other phase.

where $y_A - y_{Ai}$ and $x_{Ai} - x_A$ are concentration driving forces, k_G is the gas-phase mass transfer coefficient, and k_L is the liquid-phase mass transfer coefficient.

Mass transfer rates may also be expressed in terms of an overall gas-phase driving force by defining a hypothetical equilibrium mole fraction y^*_A as the concentration which would be in equilibrium with the bulk liquid concentration ($y^*_A = mx_A$):

$$N_A = K_{OG} P(y_A - y^*_A) \tag{6}$$

The relationship of the overall gas-phase mass transfer coefficient K_{OG} to the individual film coefficients may be found from equations 4 and 5, assuming a straight equilibrium line:

$$N_A = k_G P(y_A - y_{Ai}) = k_L \bar{\rho} \frac{1}{m} (y_{Ai} - y^*_A)$$

and by comparison with equation 6,

$$\frac{1}{K_{OG}} = \frac{1}{k_G} + \frac{mP}{k_L \bar{\rho}} \tag{7}$$

Expressions similar to equations 6 and 7 may be derived in terms of an overall liquid-phase driving force. Equation 7 represents an addition of the resistances to mass transfer in the gas and liquid films. The analogy of this process to the flow of electrical current through two resistances in series has been analyzed (43).

A representation of the various concentrations and driving forces in a y–x diagram is shown in Figure 7. The point representing the interfacial

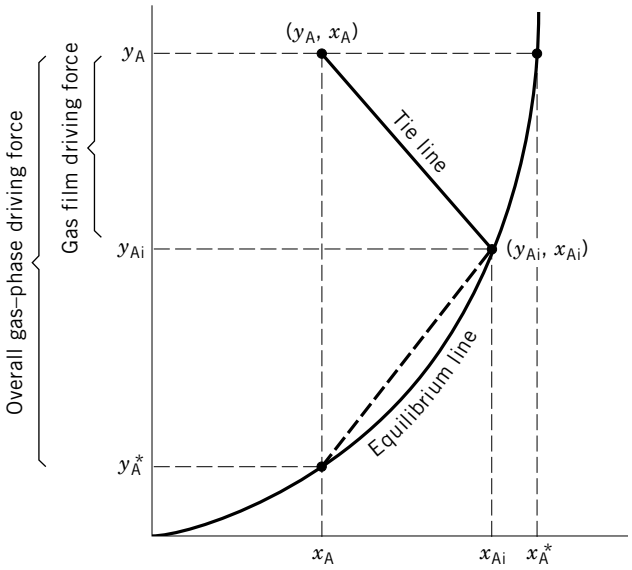

Fig. 7. The driving forces in the y–x diagram.

concentrations (y_{Ai}, x_{Ai}) must lie on the equilibrium curve since these concentrations are at equilibrium. The point representing the bulk concentrations (y_A, x_A) may be anywhere above the equilibrium line for absorption or below it for desorption. The slope of the tie line connecting the two points is given by equations 4 and 5:

$$\frac{y_A - y_{Ai}}{x_A - x_{Ai}} = -\frac{k_L \bar{\rho}}{k_G P} \tag{8}$$

In situations where the gas film resistance is predominant (gas film-controlled situation), $k_G P$ is much smaller than $k_L \rho$ and the tie line is very steep. y_{Ai} approaches y^* so that the overall gas-phase driving force and the gas-film driving force become approximately equal, whereas the liquid-film driving force becomes negligible. From equation 7, it also follows that in such cases $K_{OG} \approx k_G$. The reverse is true if the liquid film resistance is controlling. Since the example depicted in Figure 4 involves a strongly curved equilibrium line, equation 7 is only valid if the slope of the dashed line between x_A and x_{Ai} is substituted for m. Overall mass transfer coefficients may vary considerably over a certain concentration range as a result of variations in m even if the individual film constants stay essentially constant.

3.2. Mass Transfer Coefficients and Molecular Diffusion. Many theories have been put forth to explain experimentally measured mass transfer coefficients and to link them to more fundamental phenomena and parameters. There are two mechanisms that contribute to mass transfer and are reflected in the mass transfer coefficients. As described above (Fig. 6) at some distance from the interface molecules are transported towards or away from the interface mainly by turbulent convection, whereas molecular diffusion dominates mass transfer increasingly as these molecules approach the interface more closely. For analyzing the effects of molecular diffusion it is best to separate it conceptually from turbulent convection by approximating the real situation at the interface by hypothetical stagnant gas and liquid films. This model is proposed by the film theory (see below). The fluid is assumed to be essentially stagnant within these "effective" films making a sharp change to totally turbulent flow where the film is in contact with the bulk of the fluid. As a result, mass is transferred through the effective films only by steady-state molecular diffusion and it is possible to compute the concentration profile through the films by integrating Fick's law:

$$J_A = -D_{AB} \frac{dc_A}{dz} \tag{9}$$

where J_A is the flux of component A relative to the average molar flow of the whole mixture, D_{AB} is the diffusion coefficient of A in B, z is the distance of diffusion, and c_A is the molar concentration of A at a given point in the film. The bulk concentrations are denoted y_{Ab} and x_{Ab} in the following three sections whereas y_A and x_A stand for the concentration at a particular point within the films.

Equimolar Counterdiffusion in Binary Cases. If the flux of A is balanced by an equal flux of B in the opposite direction (frequently encountered in binary distillation columns), there is no net flow through the film and N_A, like J_A, is

directly given by Fick's law. In an ideal gas, where the diffusivity can be shown to be independent of concentration, integration of Fick's law leads to a linear concentration profile through the film and to the following expression where $(P/RT)y_A$ is substituted for c_A:

$$N_A = \frac{D_{AB}P}{z_0RT}(y_{Ab} - y_{Ai}) \tag{10}$$

thus

$$k_G^0 = \frac{D_{AB}}{z_0RT} \tag{11}$$

where k_G is labeled with a zero to indicate equimolar counterdiffusion and z_0 is the effective film thickness. This same treatment is usually adopted for liquids, although the diffusion coefficients are customarily not completely independent of concentration. Substituting $\overline{\rho}x_A$ for c_A, the result is

$$k_L^0 = \frac{D_A}{z_0} \tag{12}$$

Equations 11 and 12 cannot be used to predict the mass transfer coefficients directly, because z_0 is usually not known. The theory, however, predicts a linear dependence of the mass transfer coefficient on diffusivity.

Unidirectional Diffusion Through a Stagnant Medium in Binary Cases. An ideally simple gas absorption process involves diffusion of only one component through a nondiffusing medium, either the inert gas or the solvent. There exists a net flux of material through the film in this case, and therefore the mixture as a whole is not at rest. The total flux of A is now the sum of the flux with respect to the average flow of the mixture, that is still given by Fick's law of diffusion, plus the flux of A caused by the average bulk flow of the mixture itself:

$$N_A = J_A + y_A\sum_j N_j = -\frac{D_{AB}P}{RT}\frac{dy_A}{dz} + y_AN_A \tag{13}$$

The derivation of this result may be found in various texts (44). Rearranging and integrating equation 13 yields

$$N_A = \frac{D_{AB}P}{z_0RT}\frac{1}{y_{BM}}(y_{Ab} - y_{Ai}) \tag{14}$$

where y_{BM} is the logarithmic mean of the stagnant gas concentration through the film:

$$y_{BM} = \frac{(1 - y_{Ab}) - (1 - y_{Ai})}{\ln[(1 - y_{Ab})/(1 - y_{Ai})]} \tag{15}$$

Therefore

$$k'_G = \frac{D_{AB}}{z_0 R T y_{BM}} \tag{16}$$

For liquids,

$$k'_L = \frac{D_A}{z_0 x_{BM}} \tag{17}$$

where

$$x_{BM} = \frac{(1 - x_{Ab}) - (1 - x_{Ai})}{\ln[(1 - x_{Ab})/(1 - x_{Ai})]} \tag{18}$$

As y_{BM} and x_{BM} are smaller than unity, they predict an increase of mass transfer caused by the average bulk flow of the mixture as a whole. The effect is known as drift flux correction. The values of y_{BM} and x_{BM} are near unity for dilute mixtures.

Any Degree of Counterdiffusion in Binary Cases. In cases where counterdiffusion is not exactly equimolar nor zero, but somewhere in between or even outside these two cases, the influence of bulk flow of material through the films may be corrected for by the film factor concept (45). It is based on a slightly different form of equation 13:

$$N_A = J_A + y_A t_A N_A \tag{19}$$

where

$$t_A \equiv \frac{\sum_j N_j}{N_A} \tag{20}$$

Applying the same derivation as for unidirectional diffusion through a stagnant medium, the results turn out to be

$$k_G = \frac{D_{AB}}{z_0 R T Y_f} \tag{21}$$

$$k_L = \frac{D_{AB}}{z_0 X_f} \tag{22}$$

where

$$Y_f \equiv \frac{(1 - t_A y_{Ab}) - (1 - t_A y_{Ai})}{\ln(1 - t_A y_{Ab})/(1 - t_A y_{Ai})} \tag{23}$$

$$x_f \equiv \frac{(1 - t_A x_{Ab}) - (1 - t_A x_{Ai})}{\ln(1 - t_A x_{Ab})/(1 - t_A x_{Ai})} \tag{24}$$

The parameters Y_f and X_f are called the film factors. They are generalized y_{BM} and x_{BM} factors, respectively, and are reduced to them in the case of unidirectional diffusion through a stagnant medium because $t_A = 1$ in this case. The film factors Y_f and X_f correct the mass transfer coefficients for the effect of net flux, or the drift flux, through the films. In situations having strong counterdiffusion giving rise to a net flow opposed to the diffusion of A, the film factor becomes larger than one and therefore decreases the mass transfer coefficient and the flux of A. For weak or negative counterdiffusion producing a bulk flux parallel to the diffusion of A, the film factor is smaller than unity and thus increases N_A. In extreme situations, counterdiffusion may become large enough to reverse the direction of transport of a given component and force it to diffuse against its own driving force. These situations are characterized by a negative film factor, and hence a negative k_G. If equimolar counterdiffusion prevails, t_A becomes zero, the film factor is unity, irrespective of the concentration, and $k_G = k_G{}^0$.

Except for equimolar counterdiffusion, the mass transfer coefficients applicable to the various situations apparently depend on concentration through the y_{BM} and Y_f factors. Instead of the classical rate equations 4 and 5, containing variable mass transfer coefficients, the rate of mass transfer can be expressed in terms of the constant coefficients for equimolar counterdiffusion using the relationships

$$k_G Y_f = k'_G y_{BM} = k^0_G \tag{25}$$

$$k_L X_f = k'_L x_{BM} = k^0_L \tag{26}$$

This leads to rate equations with constant mass transfer coefficients, whereas the effect of net transport through the film is reflected separately in the y_{BM} and Y_f factors. For unidirectional mass transfer through a stagnant gas the rate equation becomes

$$N_A = k^0_G P(y_{Ab} - y_{Ai}) \frac{1}{y_{BM}} \tag{27}$$

For any degree of counterdiffusion,

$$N_A = k^0_G P(y_{Ab} - y_{Ai}) \frac{1}{Y_f} \tag{28}$$

Equation 28 and its liquid-phase equivalent are quite general. Similarly, the overall mass transfer coefficients may be made independent of the effect of drift flux through the films and thus nearly concentration independent for straight equilibrium lines:

$$N_A = K^0_{OGP}(y_{Ab} - y^*_A) \frac{1}{y^*_{BM}} \tag{29}$$

$$= K^*_{OGP}(y_{Ab} - y^*_A) \frac{1}{Y^*_f} \tag{30}$$

where the logarithmic means in y^*_{BM} and Y^*_f must be taken between y_{Ab} and y^*_A.

3.3. Fundamental Description of Multicomponent Diffusion using Maxwell-Stefan Equations. Fick's law cannot describe multicomponent diffusion because it links the driving force for diffusion of a given species to one single flux. If a driving force in terms of chemical potential gradient for a given species exists in a multicomponent mixture, it will cause this species to move relative to all other types of molecules in the mixture. It is not an absolute flux, as stipulated by Fick's law, but the movements of solute molecules A relative to all the other molecules j that dissipate Gibbs energy (see eq. 31). It is therefore necessary to sum over all these relative movements. Each one of them will need an amount of driving force determined by the importance of the interactions between molecules A and j, expressed by the ratio of RT and the binary diffusion coefficient A-j. The correct sum over all individual relative movements has already been worked out a long time ago and is known as the Maxwell-Stefan equations (44,46):

$$-\frac{d\mu_{\mathrm{A}}}{dz} = \sum_{j=B}^{n} \frac{RT}{D_{Aj}}\, x_j\, (U_A - U_j) \tag{31}$$

where U_j is the moving velocity of the ith species and D_{Aj} the binary diffusion coefficient between A and the jth other species in the mixture. As the Maxwell-Stefan equations are about binary interactions, there are only $n-1$ independent such equations in a n species mixture. In order to calculate all the n diffusion velocities U_{i}, one more constraint must be formulated in terms of a velocity balance such as $\Sigma\, U_i = 0$, $U_{\mathrm{B}} = 0$ or the like. After transforming the gradient of chemical potential into a mole fraction gradient and by linking U_{A} to the fluxes by $N_A = U_A \bar{\rho} x_A$ the Maxwell-Stefan equations may be written as

$$-\Gamma\, \frac{dx_A}{dz} = \sum_{j=B}^{n} \frac{N_A x_j - N_j x_A}{D_{Aj}\rho} \tag{32}$$

where

$$\Gamma = 1 + x_A\, \frac{d\ln\gamma_A}{dx_{\mathrm{A}}} \tag{33}$$

Γ is called the thermodynamic correction factor and reduces to unity for ideal mixtures. It is easily shown that for ideal binary situations equation 32 reduces to either Fick's law, equation 13 or 19 if $N_{\mathrm{B}} = -N_{\mathrm{A}}$, $N_{\mathrm{B}} = 0$, or $\Sigma\, N_{\mathrm{i}} = N_{\mathrm{A}} + N_{\mathrm{B}} = t_{\mathrm{A}} N_{\mathrm{A}}$ are substituted, respectively.

Using Maxwell-Stefan equations instead of Fick's law has the advantage of taking all the binary diffusional interactions correctly into account. The Maxwell-Stefan diffusivities can be measured in binary diffusion experiments and for gaseous mixtures are concentration independent. Another important advantage is the fact that thermodynamic nonidealities are explicitely accounted for, whereas Fick's law lumps them into the diffusion coefficient, which therefore depends more on concentration than Maxwell-Stefan diffusivities. Maxwell-Stefan equations may also readily be extended to cases where diffusion is also

driven by forces other than concentration gradients, such as pressure gradients, centrifugal force and electrical fields.

On the other hand, Maxwell-Stefan equations are not easy to integrate in order to find the concentration profiles. The fact that they are implicit in the fluxes further complicates all numerical calculations.

Treating Complex Mixtures as Pseudobinaries. The traditional way of dealing with multicomponent mixture has always been to describe the diffusion of any given type of molecule through the mixture by lumping all other species into a single pseudospecies and to compute the diffusion flux based on Fick's law. This procedure requires evaluating an effective diffusivity of A through the rest of the mixture. Eliminating the mole fraction gradient from Fick's law and from the Maxwell-Stefan equation one finds the effective diffusivity to be

$$D_{\mathrm{A_{eff}}} = \frac{N_A}{\sum_{j=B}^{n} \frac{N_A x_j - N_j x_A}{D_{Aj}}} \tag{34}$$

Effective diffusivities calculated in this way do already contain the drift-flux correction. They may be positive or negative. In general cases, they are too difficult to compute to be of practical use.

There are, however, several situations frequently occurring in practice in which mixtures do indeed behave like binaries. The most obvious case is a dilute mixture of solutes in a carrier gas or solvent, as often occurring in gas absorption. If the mole fractions of all solutes are small, the sum in equation 31 will contain only a single interaction term and equation 32 reduces to

$$-\frac{dx_{\mathrm{A}}}{dz} = \frac{N_{\mathrm{A}} x_{\mathrm{B}}}{d_{\mathrm{AB}} \rho} \tag{35}$$

Where the subscript B denotes the solvent or carrier. In this case, the Maxwell-Stefan approach for multicomponent mixtures reduces to the familiar equations treated earlier. In case x_{B} is sufficiently close to unity, equation 35 corresponds to Fick's law for equimolar counterdiffusion and the mass transfer coefficients may be evaluated as shown by equations 11 and 12. If x_{B} deviates sufficiently from unity to induce a drift flux, equation 35 reduces with $x_{\mathrm{B}} = 1 - x_{\mathrm{A}}$ to the liquid equivalent of equation 13 and the drift flux may be corrected as shown by equation 27.

Another frequently occuring case is the diffusion of a solute through a mixture of nondiffusing substances such as air. In this case, the effective diffusivity becomes

$$D_{\mathrm{A_{eff}}} = \frac{1}{\sum_{j=\mathrm{B}}^{n} \frac{x_j}{D_{\mathrm{Aj}}}} \tag{36}$$

$D_{\mathrm{A_{eff}}}$ represents the average diffusivity of A through the stagnant mixture and can directly be used in Fick's law. Mixtures in which the binary diffusion coefficients of one of the constituents are markedly lower than the others, also

may be described as pseudobinaries because only the interactions with this particular component need to be accounted for and all other terms can be neglected in equation 32. However, the evaluation of $D_{A_{eff}}$ from equation 34 remains intricate.

Other Ways to Use Maxwell-Stefan Equations. Wesselingh and Krishna (47) have proposed to integrate the Maxwell-Stefan equations by assuming linear concentration profiles through the diffusion film (eq. 37).

$$\frac{\Delta x_A}{z_o} = \sum_{j=B}^{n} \frac{N_A \bar{x}_j - N_j \bar{x}_A}{D_{Aj}\rho} \tag{37}$$

Although still not explicit in the fluxes, this technique is highly useful for numerical calculations. Wesselingh and Krishna propose to use these equations, eg, in the following form:

$$\Delta x_A = \sum_{j=B}^{n} \frac{N_A \bar{x}_j - N_j \bar{x}_A}{k_{Aj}\rho} \tag{38}$$

where k_{Aj} are binary mass transfer coefficients defined as

$$k_{Aj} = \frac{D_{Aj}}{z_0} \tag{39}$$

If the molar fraction in the bulk and at the interface are known, the fluxes in a mixture containing n species may be calculated by solving $n-1$ linear equations of the type seen in equation 38 together with one mass balance constraint such as, eg, $N_B = 0$. This procedure is thus useful for obtaining an approximately correct estimation of all fluxes through a diffusion film.

Rigorous computation of multicomponent mass transfer may be achieved resorting to the text by Taylor and Krishna (48 and references cited therein). At its heart lies a matrix formulation of the generalized Maxwell-Stefan equations (49,50). This approach is quite rigorous and consistent with the thermodynamics of irreversible processes and in the case of plate columns does not rely on the use of lumped phenomenological concepts like Murphree tray efficiencies. It also eliminates the assumption of thermal equilibrium between phases at a given stage within the column. Although it has been primarily used in the design of distillation and reactive distillation columns, it is increasingly being used for the design of absorption equipment. Reference 51 is strongly recommended as a very comprehensive and up-to-date treatise on the design and calculation of absorption columns using advanced techniques. Although the complication of some of these numerical techniques precludes its use in hand calculations, these rigorous methods have already found their way into commercial flowsheet simulators.

The use of sophisticated modeling tools is warranted when large multicomponent molar fluxes or large temperature differences between phases or both (52) are expected. In the majority of industrial design cases, however, it is satisfactory to apply simpler methods of sufficient approximation.

3.4. Mass Transfer Coefficients and Convection. As explained at the beginning of the last section, many theories have been developped in attempts to model mass transfer rates under the combined effects of molecular diffusion and turbulent convection. The classical model has been the film theory (53) effectively assuming completely stagnant layers of a given thickness z_0 adjacent to the interface and a sudden change to the completely turbulent conditions prevailing in the bulk of the phase. Mass transfer is thus assumed to occur through these films only by molecular diffusion at steady state. Equations 14–30 may then used directly to correlate mass transfer coefficients and rates.

The film model has often received criticism because it appears to predict that the rate of mass transfer is directly proportional to the molecular diffusivity. This dependency is at odds with experimental data that shows the mass transfer to be proportional to the molecular diffusivity raised to an exponent which varies between 0.5 and 0.7 (54–56), and was one of the reasons why other models were developed. In spite of this criticism, the film theory continues to be used very widely in the design of gas absorption equipment.

In contrast to the film theory, other approaches assume that transfer of material does not occur by steady-state diffusion. Rather there are large fluid motions which constantly bring fresh masses of bulk material into direct contact with the interface. According to the penetration theory (57), transient diffusion proceeds from the interface into the particular element of fluid in contact with the interface. This is an unsteady state, transient process where the rate decreases with time. After a while, the element is replaced by a fresh one brought to the interface by the relative movements of gas and liquid, and the process is repeated. In order to evaluate N_A, a constant average contact time for the individual fluid elements is assumed (57). This leads to relations such as

$$k_L = 2\sqrt{\frac{D}{\pi\tau}} \tag{40}$$

If, on the other hand, it is assumed that contact times for the individual fluid elements vary at random, an exponential surface age distribution characterized by a fractional rate of renewals may be used (58). This approach is called surface renewal theory and results in

$$k_L = \sqrt{Ds} \tag{41}$$

Neither the penetration nor the several variations on the surface renewal theory can be used to predict mass transfer coefficients directly because τ and s are not normally known. Each suggests, however, that mass transfer coefficients should vary as the square root of the molecular diffusivity and thus reflects experimental data better than the film theory.

The penetration model is also superior to the film model in predicting the influence of thermodynamic nonidealities on gas–liquid mass transfer (59). In the case of gas absorption in dilute systems, these differences are irrelevant because both transport models lead to the same expression for the transport rate as a function of the concentration difference. But in the case of gas

absorption in concentrated systems an error is introduced when the film method is used instead of the more appropriate penetration model. The mass transfer rates will be influenced by convective contributions and thermodynamic nonidealities. Mass transfer rates computed with the film method can easily differ by >50% from those obtained from the penetration model, which seems to be in better agreement with available experimental data. This criticism, while essentially correct, has been shown not to have severe consequences in practice. The simple ad hoc modification suggested in some cases (59) seems to have wide validity and does show that, for rapid design purposes, the theoretically criticized film theory can still be used very successfully.

Finally, the film-penetration theory (60) combines features of the film, penetration and surface renewal theories and predicts a dependency of the mass transfer coefficient on the diffusivity raised to a power that varies continuously between 0.5 and 1. This theory assumes the entire resistance to mass transfer to reside in a film of fixed thickness. Eddies move to and from the bulk fluid and this film. Age distributions for time spent in the film are of the Higbie (penetration) or Danckwerts (surface renewal) type. For high rates of surface renewal, it reduces to the surface renewal theory. For low rates of renewal it reduces to the film theory. Although the application of the latter theories is difficult because of lack of data on film thickness or on fractional rate of surface renewal or on both, they have found some application in the design of nonisothermal absorption with chemical reaction (61,62).

Another concept sometimes used as a basis for comparison and correlation of mass transfer data in columns is the Chilton-Colburn analogy (63). This semiempirical relationship was developed for correlating mass and heat transfer data in pipes and is based on the turbulent boundary layer model and the close analogy between momentum and mass transfer. It must be considerably modified for gas-absorption columns, but it predicts that the mass transfer coefficient varies with D raised to the two-thirds power (4,64) which is in good agreement with experimental data.

3.5. Absorption and Chemical Reaction. In instances where the solute gas is absorbed into a liquid or a solution where it is able to undergo chemical reaction, the driving forces of absorption become far more complex. The solute not only diffuses through the liquid film at a rate determined by the gradient of the concentration, but at the same time also reacts with the liquid at a rate determined by the concentrations of both the solute and the solvent at the point of interest. Calculating the concentration profiles through the liquid film requires formulating a differential mass balance over an infinitesimal control volume in the film which accounts for both diffusion and reaction of the solute gas and subsequently integrating it. The calculations show that these profiles are steeper and the rate of mass transfer higher than without chemical reaction. Thus the results are often expressed as an enhancement factor ϕ defined as the fractional increase of the liquid film mass transfer coefficient resulting from the chemical reaction (k^{r}_{L}/k^{0}_{L}). The solutions that have been developed in this manner based on the film, penetration, and surface renewal theories are quite similar for a given type of reaction (65,66). Solutions and estimations of enhancement factors may be found in the literature (4,51,65–85).

An illustration of how concentration profiles are calculated in columns for gas absorption with chemical appears at the end of the section on packed column design.

4. Design of Packed Absorption Columns

Discussion of the concepts and procedures involved in designing packed gas absorption systems shall first be confined to simple gas absorption processes without complications: isothermal absorption of a solute from a mixture containing an inert gas into a nonvolatile solvent without chemical reaction. Gas and liquid are assumed to move through the packing in a plug-flow fashion. Deviations such as nonisothermal operation, multicomponent mass transfer effects, and departure from plug flow are treated in later sections.

4.1. Standard Absorber Design Methods

Operating Line. As a gas mixture travels up through a gas absorption tower, as shown in Figure 8, the solute A is transferred to the liquid phase

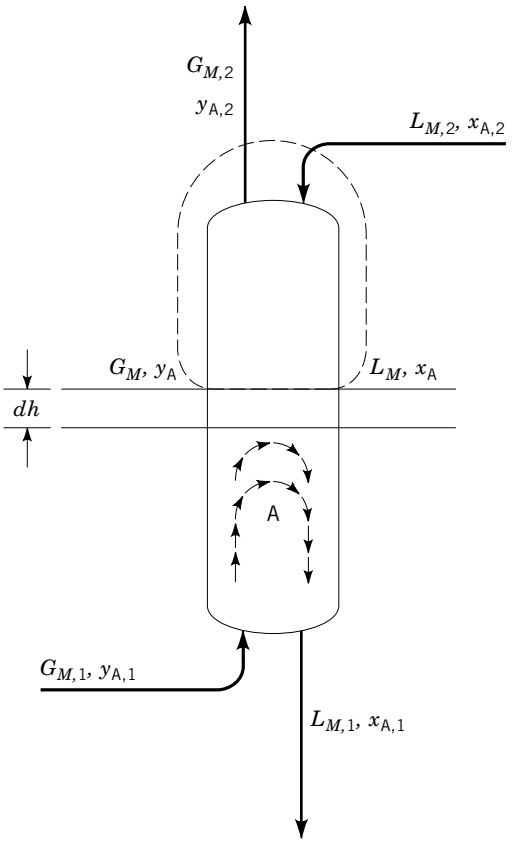

Fig. 8. Mass balance in gas absorption columns. The curved arrows indicate the travel path of the solute A. The upper broken curve delineates the envelope for the material balance of equation 42.

and thus gradually removed from the gas. The liquid accumulates solute on its way down through the column so x increases from the top to the bottom of the column. The steady-state concentrations y and x at any given point in the column are interrelated through a mass balance around either the upper or lower part of the column (eq. 43), whereas the four concentrations in the streams entering and leaving the system are interrelated by the overall material balance.

Since the total gas and liquid flow rates per unit cross-sectional area vary throughout the tower (Fig. 8) rigorous material balances should be based on the constant inert gas and solvent flow rates G'_M and L'_M, respectively, and expressed in terms of mole ratios Y' and X'. A balance around the upper part of the tower yields

$$G'_M Y' + L'_M X'_2 = G'_M Y'_2 + L'_M X' \tag{42}$$

which may be rearranged to give

$$Y' = \frac{L'_M}{G'_M}\left(X' - X'_{\mathrm{A},2}\right) + Y'_{\mathrm{A},2} \tag{43}$$

where G'_M and L'_M are in kg.mol/(h.m^2) [lb.mol/(h.ft^2)] and $Y' = y/(1-y)$ and $X' = x/(1-x)$. The overall material balance is obtained by substituting $Y' = Y'_1$ and $X' = X'_1$. For dilute gases the total molar gas and liquid flows may be assumed constant and a similar mass balance yields

$$y = \frac{L_M}{G_M}(x - x_2) + y_2 \tag{44}$$

A plot of either equation 43 or 44 is called the operating line of the process as shown in Figure 9. As indicated by equation 44, the line for dilute gases is straight, having a slope given by L_M/G_M. (This line is always straight when plotted in $Y' - X'$ coordinates.) Together with the equilibrium line, the operating line permits the evaluation of the driving forces for gas absorption along the column (Fig. 7). The farther apart the equilibrium and operating lines, the larger the driving forces become and the faster absorption occurs, resulting in the need for a shorter column (Fig. 9).

To place the operating line, the flows, composition of the entering gas y_1, entering liquid x_2, and desired degree of absorption y_2, are usually specified. The specification of the actual liquid rate used for a given gas flow (the L_M/G_M ratio) usually depends on an economic optimization because the slope of the operating line may be seen to have a drastic effect on the driving force. For example, use of a very high liquid rate (line A in Fig. 9) results in a short column and a low absorber cost, but at the expense of a high cost for solvent circulation and subsequent recovery of the solute from a relatively dilute solution. On the other hand, a liquid rate near the theoretical minimum, which is the rate at which the operating line just touches the equilibrium line (line B in Fig. 9), requires a very tall tower because the driving force becomes very small at its bottom (the extreme case in which which the operating line just touches the equilibrium line is usually designated as a “pinch point”). Use of a liquid rate on the order of one

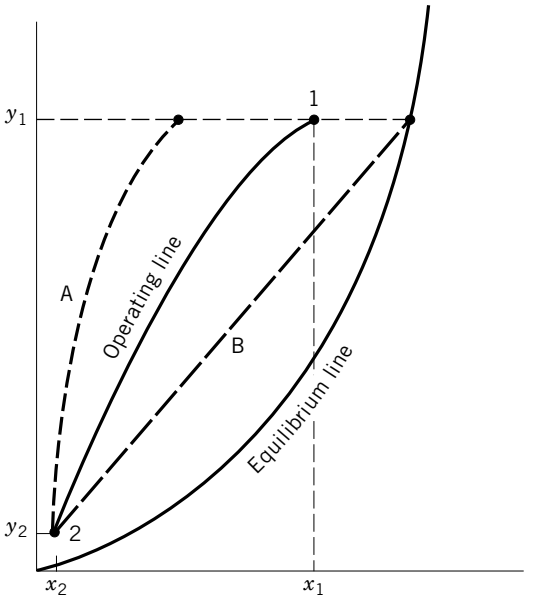

Fig. 9. Operating lines for an absorption system: line A, high L_M/G_M ratio; solid line, medium L_M/G_M ratio; line B, L_M/G_M ratio at theoretical minimum necessary for the removal of the specified quantity of solute. Subscript 1 represents the bottom of tower, 2, the top of tower.

and one-half times the theoretical minimum is not unusual. In the absence of a detailed cost analysis, the L_M/G_M ratio is often specified at 1.4 times the slope of the equilibrium line (86).

Design Procedure. The packed height of the tower required to reduce the concentration of the solute in the gas stream from $y_{A,1}$ to an acceptable residual level of $y_{A,2}$ may be calculated by combining point values of the mass transfer rate and a differential material balance for the absorbed component. Referring to a slice dh of the absorber (Fig. 8),

$$N_A a\, dh = -d(G_M y) = -G_M dy - y\, dG_M \tag{45}$$

and

$$dG_M = -N_A a\, dh \tag{46}$$

where a is the interfacial area present per unit volume of packing. Combining equations 45 and 46,

$$-dh = \frac{G_M\, dy}{N_A a(1-y)} \tag{47}$$

Substituting for N_A from equation 27 and integrating over the tower,

$$h = \int_{y_2}^{y_1} \frac{G_M}{k_G^0 a P} \frac{y_{BM}\, dy}{(1-y)(y-y_i)} \tag{48}$$

Equation 48 may be integrated numerically or graphically and its component terms evaluated at a series of points on the operating line. y_i is found by placing tie lines from each of these points; the slopes are given by equation 8. Thus equation 48 is a general expression determining the column height required to effect a given reduction in y_A.

Equation 48 can often be simplified by adopting the concept of a mass transfer unit. As explained in the film theory discussion earlier, the purpose of selecting equation 27 as a rate equation is that k_G^0 is independent of concentration. This is also true for the $G_M/k_G^0 aP$ term in equation 48. In many practical instances, this expression is fairly independent of both pressure and G_M: as G_M increases through the tower, $k^0{}_G$ increases also, nearly compensating for the variations in G_M. Thus this term is often effectively constant and can be removed from the integral:

$$h = \left(\frac{G_M}{k_G^0 a P}\right) \int_{y_2}^{y_1} \frac{y_{BM}\, dy}{(1-y)(y-y_i)} \tag{49}$$

The parameter $G_M/k^0{}_G aP$ has the dimension of length or height and is thus designated the gas-phase height of one transfer unit, H_G. The integral is dimensionless and indicates how many of these transfer units it takes to make up the whole tower. Consequently, it is called the number of gas-phase transfer units, N_G. Equation 49 may therefore be written as

$$h = (H_G)(N_G) \tag{50}$$

where

$$H_G = \frac{G_M}{k_G^0 a P} \tag{51}$$

and

$$N_G = \int_{y_2}^{y_1} \frac{y_{BM}\, dy}{(1-y)(y-y_i)} \tag{52}$$

The same treatment for the liquid side yields

$$h = (H_L)(N_L) \tag{53}$$

where

$$H_L = \frac{L_M}{k_L^0 a \bar{\rho}} \tag{54}$$

and

$$N_{\mathrm{L}} = \int_{x_2}^{x_1} \frac{x_{\mathrm{BM}}\, dx}{(1-x)(x_{\mathrm{i}}-x)} \tag{55}$$

A similar treatment is possible in terms of an overall gas-phase driving force by substituting equation 29 into equation 47:

$$h = (H_{\mathrm{OG}})(N_{\mathrm{OG}}) \tag{56}$$

where

$$H_{\mathrm{OG}} = \frac{G_M}{K^0_{\mathrm{OG}} a P} \tag{57}$$

and

$$N_{\mathrm{OG}} = \int_{y_2}^{y_1} \frac{y^*_{\mathrm{BM}}\, dy}{(1-y)(y-y^*)} \tag{58}$$

Both H_{OG} and N_{OG} are called the overall gas-phase height of a transfer unit and the number of overall gas-phase transfer units, respectively. In the case of a straight equilibrium line, K^0_{OG} is often nearly concentration-independent as explained earlier. In such cases, use of equation 56 is especially convenient because N_{OG}, as opposed to N_{G}, can be evaluated without solving for the interfacial concentrations. In all other cases, H_{OG} must be retained under the integral and its value calculated from H_{G} and H_{L} at different points of the equilibrium line as

$$H_{\mathrm{OG}} = \frac{y_{\mathrm{BM}}}{y^*_{\mathrm{BM}}} H_{\mathrm{G}} + \frac{m G_M}{L_M} \frac{x_{\mathrm{BM}}}{y^*_{\mathrm{BM}}} H_{\mathrm{L}} \tag{59}$$

To use all of these equations, the heights of the transfer units or the mass transfer coefficients $k^0_{\mathrm{L}} a$ and k^0_{L} must be known. Transfer data for packed columns are often measured and reported directly in terms of from H_{G} and H_{L} and correlated in this form against from G_M and L_M.

Sometimes the height equivalent to a theoretical plate (HETP) is employed rather than from H_{G} and H_{L} to characterize the performance of packed towers. The number of heights equivalent to one theoretical plate required for a specified absorption job is equal to the number of theoretical plates, N_{TP}. It follows that

$$h = (\mathrm{HETP})(N_{\mathrm{TP}}) \tag{60}$$

which is similar in form to equation 56. The HETP is a less fundamental variable than the heights of the transfer units, and it is more difficult to translate HETPs from one situation to another. Only for linear operating and equilibrium lines can they be related analytically to H_{OG} as shown later by equation 86.

4.2. Simplified Design Procedures for Linear Operating and Equilibrium Lines

Logarithmic-Mean Driving Force. As noted earlier, linear operating lines occur if all concentrations involved stay low. Where it is possible to assume that the equilibrium line is linear, it can be shown that use of the logarithmic mean of the terminal driving forces is theoretically correct. When the overall gas-film coefficient is used to express the rate of absorption, the calculation reduces to solution of the equation

$$L_M(x_1 - y_2) = G_M(y_1 - y_2) = K_{OG}aPh(y - y^*)_{av} \tag{61}$$

where

$$(y - y^*)_{av} = \frac{(y_1 - y_1^*) - (y_2 - y_2^*)}{\ln[(y_1 - y_1^*)/(y_2 - y_2^*)]} \tag{62}$$

In these cases, a quantitative significance can be given to the concept of a transfer unit. Because $H_{OG} = G_M/K_{OG}aP$, it follows from equations 61 and 56 that

$$N_{OG} = \frac{y_i - y_2}{(y - y^*)_{av}}$$

Therefore, in this case, one transfer unit corresponds to the height of packing required to effect a composition change just equal to the average driving force.

Number of Transfer Units. For relatively dilute systems the ratios involving y_{BM}, y_{BM}^*, and $1 - y$ approach unity so that the computation of H_{OG} from equation 59 and N_{OG} from equation 58 may be simplified to

$$H_{OG} = H_{HG} + \left(\frac{mG_M}{L_M}\right)H_L \tag{63}$$

$$N_{OG} \approx N_T = \int_{y_2}^{y_1} \frac{dy}{y - y^*} \tag{64}$$

Equation 64 is a rigorous expression for the number of overall transfer units for equimolar counterdiffusion, in distillation columns, for instance.

For cases in which the equilibrium and operating lines may be assumed linear, having slopes L_M/G_M and m, respectively, an algebraic expression for the integral of equation 64 has been developed (86):

$$N_{OG} \approx N_T = \frac{\ln\left[\left(1 - \frac{mG_M}{L_M}\right)\left(\frac{y_1 - mx_2}{y_2 - mx_2}\right) + \frac{mG_M}{L_M}\right]}{1 - \frac{mG_M}{L_M}} \tag{65}$$

The required tower height may thus be easily calculated using equation 56, where H_{OG} is given by equation 63 and N_{OG} by equation 65.

4.3. Rapid Approximate Design Procedure for Curved Operating and Equilibrium Lines. If the operating or the equilibrium line is nonlinear, equation 65 is of little use because mG_M/L_M will assume a range of values over the tower. The substitution of effective average values for m and for L_M/G_M into equations 59 and 65 obviates lengthy graphical or numerical integrations and leads to a quick, approximate solution for the required tower height (4).

The effective average values of m and L_M/G_M were determined in a computational study covering hundreds of hypothetical absorber designs for gas streams containing up to 80 mol% of solute for recoveries from 81 to 99.9%. By numerical integration, precise values were obtained for N_{OG} and N_T. By solving equation 65 numerically for each of the design cases, average values of the slope of the equilibrium line m and average flow ratios $L_M/G_M = R_{av}$ were found which gave the same N_T when substituted into equation 65 as the graphical or numerical integration.

It was found that the effective average L_M/G_M ratio, R_{av}, could be correlated satisfactorily as a function of the terminal values R_1 and R_2, of the change in the mole fraction of the absorbed component over the tower, and of the fractional approach to equilibrium y_1^*/y_1 between the concentrated gas entering the tower and the liquid leaving. Figure 10 shows the resulting correlation for cases with $L_M/G_M > 1$. No correlation was obtained when this ratio was less

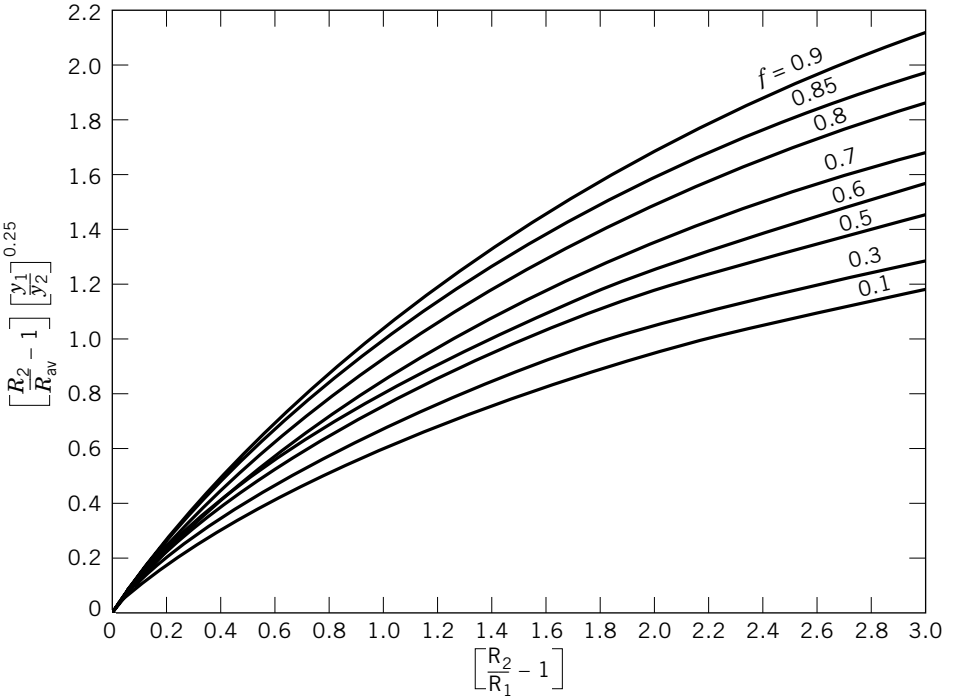

Fig. 10. Design chart for estimation of average-flow ratio in absorption (4). $R_2 = L_M/G_M$ at gas outlet; $R_1 = G_M/L_M$ at gas inlet; y_2 = mole fraction in outlet gas; y_1 = mole fraction in inlet gas; R_{av} = effective average L_M/G_M; $f = y^*_1/y_1$ = fractional approach to equilibrium.

than unity. The effective average slope of the equilibrium line, m, was correlated as a function of the initial slope m_2, of the slope m_c of the chord connecting the points on the x-y diagram with the coordinates (x_1, y_1^*) and (x_2, y_2^*), and of various other parameters as shown in Figure 11. Figure 11**a** applies when the equilibrium line is concave upward, ie, m_c/m_2; and Figure 11**b** applies when the curvature is concave downward, m_c/m_2.

The recommended design procedure uses the values of $(L_M/G_M)_{av}$ and m from Figures 10 and 11 in equation 65 and yields a very good estimation of N_T despite the curvature of the operating and the equilibrium lines. This value differs from N_{OG} obtained by equation 58 because of the $y_{BM}^*/(1-y)$ term in the latter equation. A convenient approach for purposes of approximate design is to define a correction term ΔN_{OG} which can be added to equation 64:

$$N_{OG} = N_T + \Delta N_{OG} \tag{66}$$

For cases in which y_{BM}^* may be represented by arithmetic mean (87),

$$\Delta N_{OG} = \frac{1}{2} \ln \frac{1-y_2}{1-y_1} \tag{67}$$

Equation 67 is sufficiently accurate for most situations.

The average slopes R_{av} and m from Figures 10 and 11 may also be used in equation 63 to compute H_{OG} although equation 59, with some suitable averages of y^*_{BM} and x_{BM}, should be preferred. Use of point values at an effective average liquid concentration given by equation 68 is suggested.

$$\bar{x} = \left(\frac{R_2}{R_{av}} - 1 \right) / (R_2 - 1) \tag{68}$$

In many situations, however, especially when $m > 1$, the results using the simpler equation 63 are virtually the same. The required tower height is finally calculated by means of equation 56.

4.4. Drift Flux Correction for Pseudobinary Cases

Equimolar Counterdiffusion. Just as unidirectional diffusion through stagnant films represents the situation in an ideally simple gas absorption process, equimolar counterdiffusion prevails as another special case in ideal distillation columns. In this case, the total molar flows L_M and G_M are constant, and the mass balance is given by equation 44. As shown earlier, no y_{BM} factors have to be included in the derivation and the height of the packing is

$$h_T = \int_{y_2}^{y_1} H_G \frac{dy}{y - y_i} \tag{69}$$

N_{OG} is given by N_T:

$$N_{OG} = \int_{y_2}^{y_1} \frac{dy}{y - y^*} \tag{70}$$

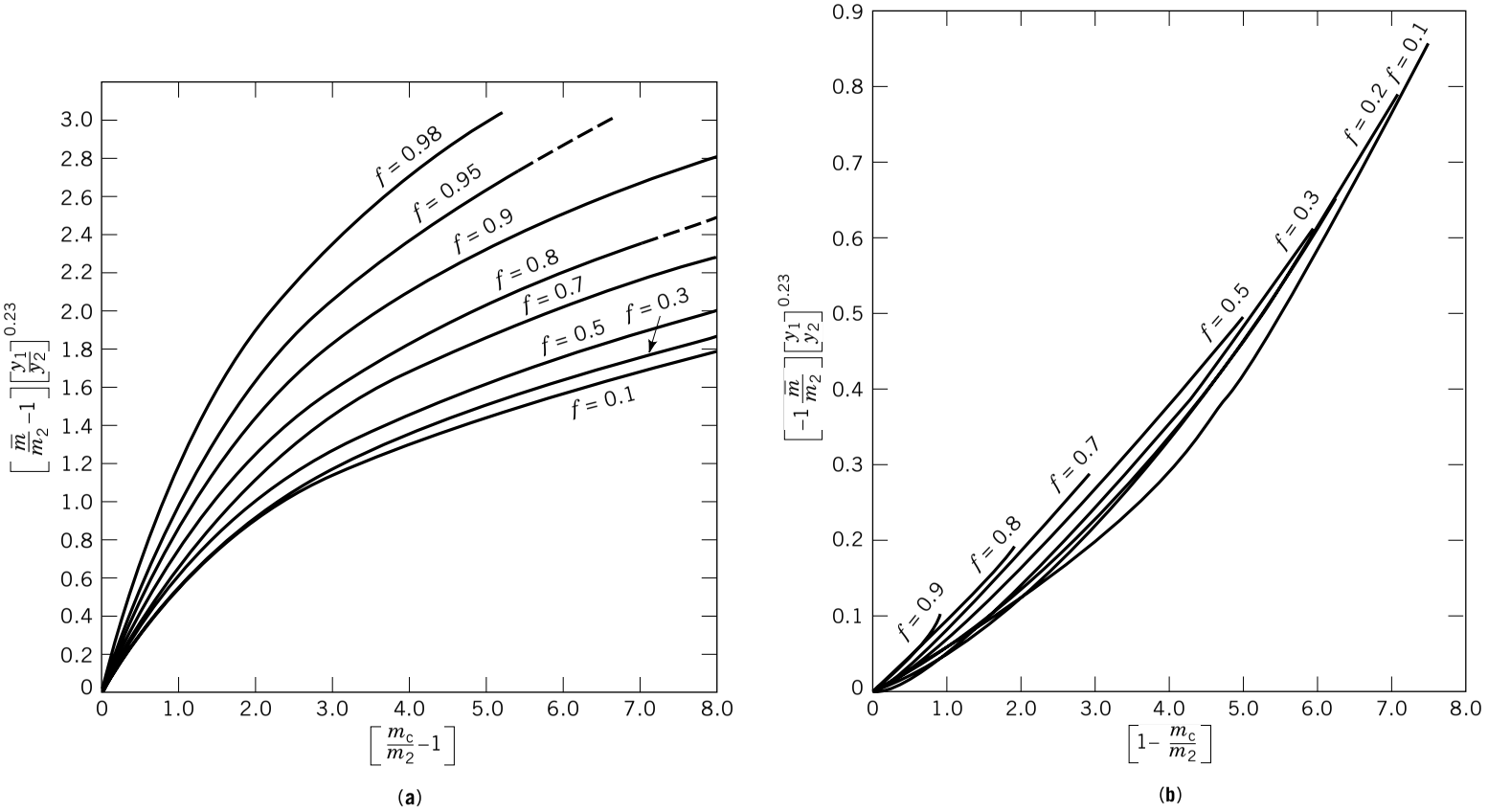

Fig. 11. Correlation of the effective average slopes m of the equilibrium line (4). (**a**) Equilibrium line curved concave upward; (**b**) equilibrium line curved concave downward.

and H_{OG} is rigorously defined by equation 63. It must, however, be retained under the integral because m usually changes over the tower:

$$h = \int_{y_2}^{y_1} H_{OG} \frac{dy}{y - y^*} \tag{71}$$

General Situation. Both unidirectional diffusion through stagnant media and equimolar diffusion are idealizations that are usually violated in real processes. In gas absorption, slight solvent evaporation may provide some counterdiffusion, and in distillation counterdiffusion may not be equimolar for a number of reasons. This is especially true for multicomponent operation.

A simple treatment is still possible if it may be assumed that the flux of the component of interest A through the interface stays in a constant proportion to the total molar transfer through the interface over the entire tower and by treating multicomponent absorption as pseudobinary cases:

$$\frac{\sum N_j}{N_A} = t_A = \text{constant} = \frac{\sum \Delta g_j}{\Delta g_A} \tag{72}$$

where Δg_j = total moles of component j absorbed over the tower. It will generally suffice to compute t_A from preliminary estimates of Δg_j and Δg_A, the total mass transfer of each component over the tower.

The mass balance for A is best represented as a straight line in hypothetical coordinates Y^0 and X^0:

$$Y_A^0 = \frac{L_M^0}{G_M^0}\left(X_A^0 - X_{A,2}^0\right) + Y_{A,2}^0 \tag{73}$$

where $Y^0{}_A = y_A/(1 - t_A y_A)$, $X^0{}_A = x_A/(1 - t_A x_A)$, $G^0{}_M = G_M/(1 - t_A y_A)$, and $L^0{}_M = L_M/(1 - t_A x_A)$, $G^0{}_M$ and $L^0{}_M$ are always constant, whereas G_M and L_M are not. For unimolecular diffusion through stagnant gas ($t_A = 1$), Y^0 and X^0 reduce to Y' and X' $G^0{}_M$ and $L^0{}_M$ reduce to G'_M and L'_M; equation 73 then becomes equation 43. For equimolar counterdiffusion $t_A = 0$, and the variables reduce to y, x, G_M and L_M, respectively, and equation 73 becomes equation 44 . Using the film factor concept and rate equation 28, the tower height may be computed by

$$h_T = \int_{y_2}^{y_1} H_G \frac{Y_f}{(1 - t_A y_A)} \frac{dy_A}{(y_A - y_{Ai})} \tag{74}$$

y_{Ai} is found as usual through tie lines of the slope

$$\frac{y_A - y_{Ai}}{x_A - x_{Ai}} = -\frac{L_M}{G_M}\frac{H_G}{H_L}\frac{Y_f}{X_f} \tag{75}$$

where

$$\frac{L_M}{G_M} = \frac{L_M^0(1 - t_A y_A)}{G_M^0(1 - t_A x_A)} \tag{76}$$

It may be noted that the above system of equations is quite general and encompasses both the usual equations given for gas absorption and distillation as well as situations with any degree of counterdiffusion. The exact derivations may be found elsewhere (4). The system of equation is, however restricted to cases that may be treated as pseudo binary (see Section 3.3).

4.5. Nonisothermal Gas Absorption

Nonvolatile Solvents. In practice, some gases tend to liberate such large amounts of heat when they are absorbed into a solvent that the operation cannot be assumed to be isothermal, as has been done thus far. The resulting temperature variations over the tower will displace the equilibrium line on a $y-x$ diagram considerably because the solubility usually depends strongly on temperature. Thus nonisothermal operation affects column performance drastically.

The principles outlined so far may be used to calculate the tower height as long as it is possible to estimate the temperature as a function of liquid concentration. The classical basis for such an estimate is the assumption that the heat of solution manifests itself entirely in the liquid stream. It is possible to relate the temperature increase experienced by the liquid flowing down through the tower to the concentration increase through a simple enthalpy balance, equation 77, and thus correct the equilibrium line in a $y-x$ diagram for the heat of solution as shown in Figure 12,

$$T_{\mathrm{L}} \approx T_{\mathrm{L2}} + \frac{(x_{\mathrm{A}} - x_{\mathrm{A2}})H_{\mathrm{OS}}}{x_{\mathrm{A}}C_{\mathrm{qA}} + (1 - x_{\mathrm{A}})C_{\mathrm{qB}}} \tag{77}$$

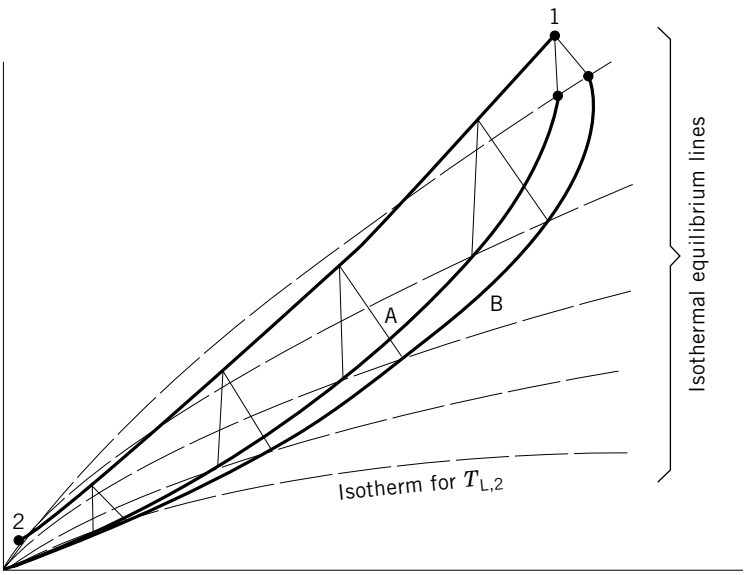

Fig. 12. Simple model of adiabatic gas absorption. (A) nonisothermal equilibrium line for overall gas-phase driving force: $y^* = f(x, T_{\mathrm{L}})$; (B) nonisothermal equilibrium line for individual gas-film driving force: $y_{\mathrm{i}} = f(x_{\mathrm{i}})$.

where T_L is the liquid temperature, °C; T_{L2} is the temperature of the entering liquid, °C; C_{qj} is the liquid molar heat capacity of component j; H_{OS} is the integral mean heat of solution of solute. For each pair of values for x_A and T_L obtained from equation 68 it is possible to evaluate $y^*(x, T_L)$, the concentration in equilibrium with the bulk of the liquid phase, and to place the equilibrium line for the overall driving force (Fig. 12A). The line connecting the actual interfacial concentrations (y_i, x_i), Figure 12B, does not coincide with line A unless there is no liquid mass transfer resistance. However, because the interfacial temperature T_i and the bulk liquid temperature T_L usually are virtually equal, the equilibrium concentration y^* and the actual interfacial concentration y_i are connected by an isotherm. Line B may therefore be constructed as shown on the basis of line A, tie lines, and isothermal equilibrium lines. Line B may be used in conjunction with equation 48 to compute the required depth of packing.

General Case. The simple adiabatic model just discussed often represents an oversimplification, since the real situation implies a multitude of heat effects: (*1*) The heat of solution tends to increase the temperature and thus to reduce the solubility. (*2*) In the case of a volatile solvent, partial solvent evaporation absorbs some of the heat. (This effect is particularly important when using water, the cheapest solvent.) (*3*) Heat is transferred from the liquid to the gas phase and vice versa. (*4*) Heat is transferred from both phase streams to the shell of the column and from the shell to the outside or to cooling coils.

In the general case, the temperature profile is determined simultaneously by all of the four heat effects. The temperature influences the transfer of mass and heat to a large extent by changing the solubilities. This turns the simple gas absorption process into a very complex one and all factors exhibit a high degree of interaction. Computer algorithms for solving the problem rigorously have been developed (51,88,89) and several implementations are available in kinetic or rate-based column modules in flowsheet simulators . Figure 13 depicts typical profiles through an adiabatic packed gas absorber from one of these algorithms (88,89). The calculations were carried out to solve a design example calling for the removal of 90% of the acetone vapors present in an air stream by absorption into water at an L_M/G_M ratio of 2.5. The air stream contained 6 mol % acetone and was saturated with water; the ambient temperature was 15°C.

It is a typical feature of such calculations that the shapes of the liquid temperature profiles are highly irregular and often exhibit maxima within the column. Such internal temperature maxima have been observed experimentally in plate and packed absorbers (88,90,91), and the measured temperature profiles can be shown to agree closely with rigorous computations. The appearance of an internal hot spot (and eventually an internal pinch-point) in the absorber is relatively common in natural gas sweetening with amines and in the absorption of water vapor from air with organic salts of alkali metals. The temperature maximum occurs in part because the heat of solution causes the entering liquid stream to be heated. In the lower part of the tower, however, the heat of absorption is smaller than the opposite heat effects of solvent evaporation and heat transfer to the cold entering gas, so that the net effect is a cooling of the liquid phase. These transfers are reversed in the upper part of the column, as is obvious from Figure 13: The gas gives up heat to the liquid, is cooled, and some of the solvent condenses from the gas stream into the liquid stream, which is heated

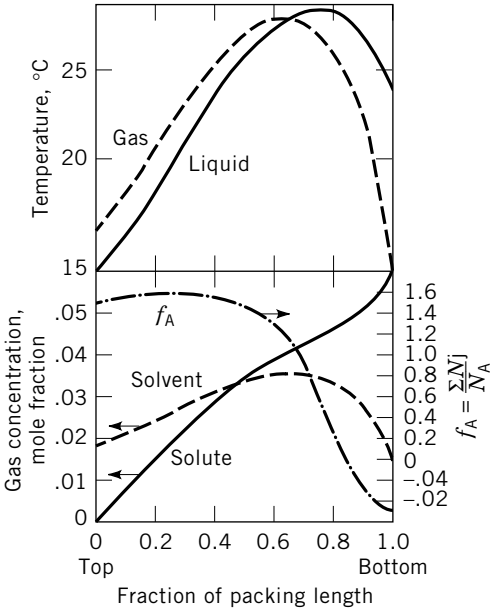

Fig. 13. Computed rigorous profiles through an adiabatic packed absorber during the absorption of acetone into water (89).

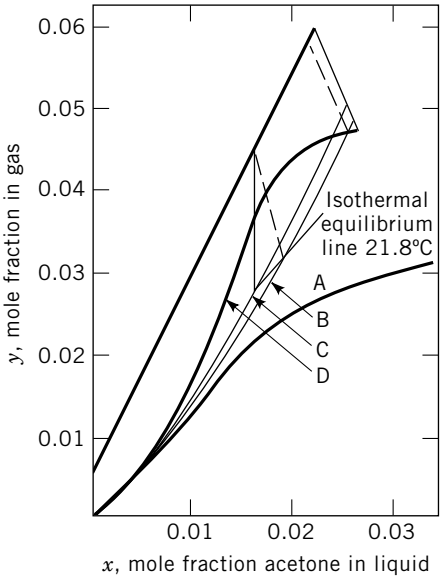

Fig. 14. The $y - x$ diagram for adiabatic absorption of acetone into water. (A) isothermal equilibrium line at T_{L2}; (B) equilibrium line for simple model of adiabatic gas absorption, gas-film driving force; (C) equilibrium line for simple model of adiabatic gas absorption, overall gas-phase driving force; (D) rigorously computed equilibrium line, gas-film driving force (89).

Table 2. **Comparison of Results of Different Design Calculations**

Method used	N_{OG}	Required depth of packing, m
rigorous calculation	5.56	3.63
isothermal approximation	3.30	1.96
simple adiabatic model	4.01	2.38

much faster in this part of the column than would be the case with the absorption alone. Figure 14 shows the rigorously computed $y-x$ diagram for the same example. The temperature maximum within the column produces a region of reduced solubility reflecting itself in the typical bulge in the middle of the rigorous equilibrium line. Since less acetone is absorbed in this part of the equipment, the gas concentration curve exhibits a slight plateau (Fig. 13). This example may also serve as a demonstration of the difficulty in estimating the required depth of packing using simplifying assumptions (Table 2). The isothermal approximation failed completely in this case and yielded 1.95 m of required packing as opposed to the rigorously determined value of 3.63 m. Neglecting the temperature increase completely, this model assumes a solubility which is much too large, reflected by equilibrium line A, and thus underestimates the rigorous result by 90%.

The standard way to correct for the heat of solution approximately is the simple adiabatic model described on the preceding pages, which yields equilibrium line B if the gas-phase driving force is used and line C on the basis of the overall driving force. This model, however, is a poor representation of the conditions prevailing in the absorber, as demonstrated by the deviation of its equilibrium line B from the rigorous line D. The approximation underestimates the true packing depth value of 3.63 m by more than one-third yielding 2.4 m (Table 2).

These calculations emphasize how important it is to account for heat effects even when performing quick, preliminary calculations. Since correct numerical calculations are not quite straightforward due to the highly non-linear character of the problem, a rapid approximate design procedure has been developped permitting to assess the importance of deviations from isothermal conditions without the need to resort to a computer (6,92).

4.6. Axial Dispersion Effects

Effect of Axial Dispersion on Column Performance. Another assumption underlying standard design methods is that the gas and the liquid phases move in plug-flow fashion through the column. In reality, considerable departure from this ideal flow assumption exists (4) and different fluid particles travel through the packing at varying velocities. The impact of this effect, which is usually referred to as axial dispersion, on the concentration profiles is demonstrated in Figure 15. The effect counteracts the countercurrent contacting scheme for which the column is designed and thus lowers the driving forces throughout the packed bed. Neglect of axial dispersion results in an overestimation of the driving forces and in an underestimation of the number of transfer units needed. It may therefore lead to an unsafe design.

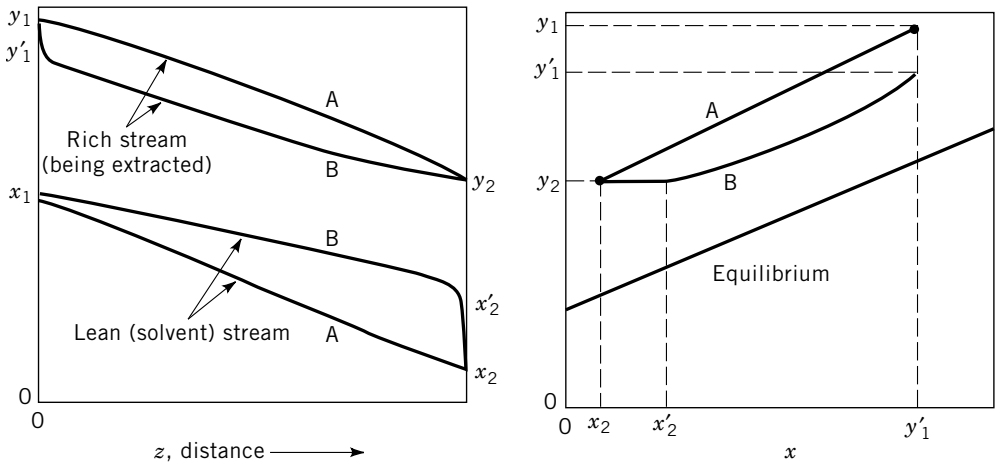

(**a**) Concentration distribution (**b**) Operating diagram

Fig. 15. Effect of axial dispersion in both phases on solute distribution through countercurrent mass transfer equipment. A, piston or plug flow; B, axial dispersion in both streams (diagrammatic). Reprinted with permission (4).

Determination of separation efficiencies from pilot-plant data is also affected by axial dispersion. Neglecting it yields high H_G or H_L values. Literature data for this parameter have usually not been corrected for this effect.

The extent of axial dispersion occurring in a gas absorber can be determined by measuring the residence time distribution of both gas and liquid. Based on classical flow models of axial dispersion, the result is usually expressed in terms of two Peclet numbers (Pe), one for each phase. Peclet numbers tending towards infinity indicate near-ideal plug flow, whereas vanishing values of Pe indicate axial dispersion to such an extent that the phase begins to become well back-mixed. When designing packed columns, the Peclet numbers are usually estimated from literature correlations (93–95). Correlations for predicting Peclet numbers in large scale gas-liquid contactors are quite scarce, but contributions have been made (96–100). Some of the available data have been described (4) and a review of published correlations for liquid-phase Peclet numbers is also available (100). Figure 16 reproduces some data (96). Axial dispersion data for bubble columns and other less common systems have also been published (101–105).

When designing packed towers, axial dispersion can be accounted for by incorporating terms for axial dispersion of the solute into the differential mass balance equation 45. The integration of the resulting differential equations is best effected by computer. Analytical solutions for cases having linear equilibrium and operating lines have been developed (106,107). They are, however, not explicit for the design case and are of such complexity that application for design also requires a computer.

Rapid Approximate Design Procedure. Several simplified approximations to the rigorous solutions have been developed over the years (101–105,107–110),

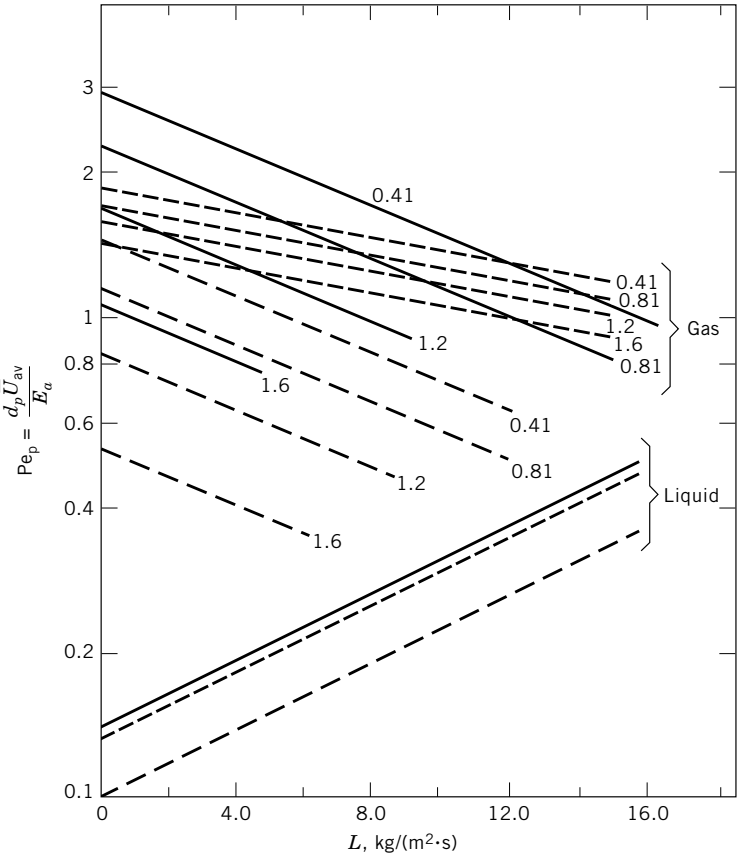

Fig. 16. Peclet numbers in large scale gas–liquid contactors using 2.54-cm Berl saddles (—) or 2.54 cm (– –) or 5.08 cm (– – –) Raschig rings (96). Numbers on lines represent G values = gas flow in kg/(m^2·s); d_p = nominal packing size; U_{av} = superficial velocity. To convert kg/(m^2·s) to lb/(h-ft^2) multiply by 737.5. Reprinted with permission (4).

but they all remain too complicated for practical use. A simple method proposed in 1989 (111,112) uses a correction factor accounting for the effect of axial dispersion, which is defined as (107)

$$\text{correction factor} = \frac{\mathrm{NTU_{ap}}}{\mathrm{NTU}} \tag{78}$$

The parameter $\mathrm{NTU_{ap}}$ is the "exterior apparent" overall gas-phase number of transfer units calculated neglecting axial dispersion simply on the basis of equation 65, whereas NTU stands for the higher real number of transfer units (N_{OG}) which is actually required under the influence of axial dispersion. The correction

factor ratio can be represented as a function of those parameters that are actually known at the outset of the calculation

$$\frac{\mathrm{NTU_{ap}}}{\mathrm{NTU}} = f\left(\mathrm{NTU_{ap}}, \left(\frac{mG}{L}\right), \mathrm{Pe}_x, \mathrm{Pe}_y\right) \tag{79}$$

Equation 79 is shown graphically in Figure 17**a** for a given set of conditions. Curves such as these cannot be directly used for design, however, because the Peclet number contains the tower height h as a characteristic dimension. Therefore, new Peclet numbers are defined containing H_{OG} as the characteristic length. These relate to the conventional Pe as

$$\mathrm{Pe_{HTU}} = \frac{uH_{\mathrm{OG}}}{D_{\mathrm{ax}}} = \frac{uh}{D_{\mathrm{ax}}}\ \frac{H_{\mathrm{OG}}}{h}$$

$$= \mathrm{Pe}\frac{1}{N_{\mathrm{OG}}} \tag{80}$$

The correction factor $(\mathrm{NTU})_{\mathrm{ap}}/\mathrm{NTU}$ as a function of $\mathrm{Pe_{HTU}}$ rather than Pe is shown in Figure 17**b**. The correction factors given in Figures 17**a** and 17**b** can roughly be estimated as

$$\frac{\mathrm{NTU_{ap}}}{\mathrm{NTU}} \approx 1 - \frac{\mathrm{NTU_{ap}}}{\dfrac{\ln S}{S-1} + \dfrac{\mathrm{Pe}_x\mathrm{Pe}_y}{\mathrm{Pe}_y + S\mathrm{Pe}_x}} \tag{81}$$

$$\frac{\mathrm{NTU_{ap}}}{\mathrm{NTU}} \approx \frac{\mathrm{Pe_{HTU,}}_y\mathrm{Pe_{HTU,}}_x}{\mathrm{Pe_{HTU,}}_y\mathrm{Pe_{HTU,}}_x + \mathrm{Pe_{HTU,}}_y + S\mathrm{Pe_{HTU,}}_x} \tag{82}$$

In these equations, S denotes the stripping factor, mG_M/L_M. Equation 82 is only valid for a sufficiently high number of transfer units so that the correction factor becomes independent of $\mathrm{NTU_{ap}}$.

In the original study (111), $\mathrm{NTU_{ap}}/\mathrm{NTU}$ was calculated for thousands of hypothetical design cases as a function of both Pe and $\mathrm{Pe_{HTU}}$. The results were correlated and empirical expressions were given that can be evaluated on a handheld calculator, just as equations 81 and 82, but which approximate the computer calculation much better, to within about +/− 5%.

The recommended rapid design procedure consists of the following steps: (*1*) The apparent N_{OG} is calculated using equation 65. (*2*) The extent of axial dispersion is estimated from literature correlations for each phase in terms of Pe numbers and transformed into $\mathrm{Pe_{HTU}}$ values. (*3*) The correction factor $\mathrm{NTU_{ap}}/\mathrm{NTU}$ is estimated on the basis of the correlation given in the literature (111). A reasonable, conservative estimate may also be obtained using equation 82, provided $\mathrm{NTU_{ap}} > 5$. When the apparent number of transfer units is divided by this correction factor, the value of N_{OG} actually required under the influence of axial dispersion is obtained. (*4*) The packed tower height is found by multiplying N_{OG} by the true $\mathrm{H_{OG}}$. In order to obtain values for the latter, pilot-plant data has to be

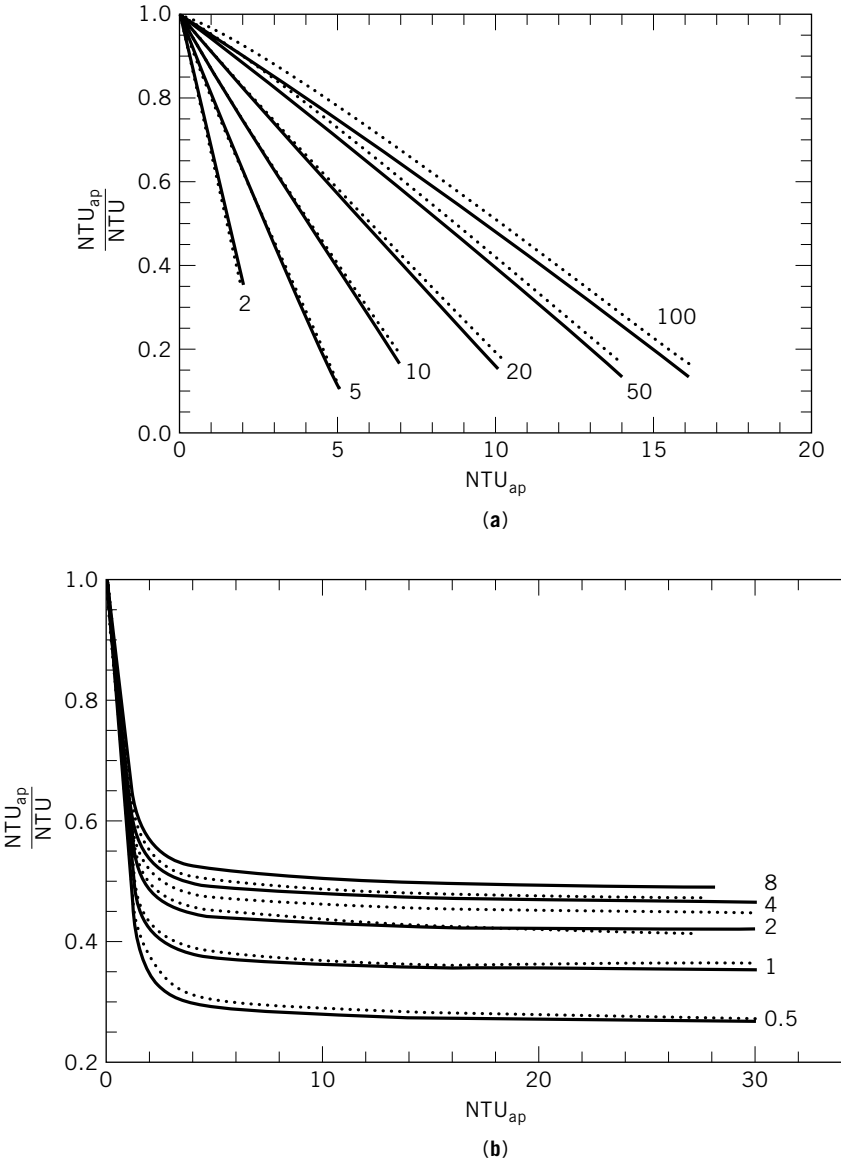

Fig. 17. Correction factor for axial dispersion as a function of NTU_{ap}. Solid lines are rigorous calculations; broken lines, approximate formulas according to literature (111). (**a**) Numbers on lines represent Pe_x values; $Pe_y = 20$; $mG_M/L_M = 0.8$. (**b**) For design calculations. Numbers on lines represent $Pe_{HTU,x}$ values; $Pe_{HTU,y} = 1$; $mG_M/L_M = 0.8$.

corrected for the influence of axial dispersion. This correction may be made in a manner similar to that described above, but equation 81 would be used to estimate the correction factor rather than equation (82).

4.7. Experimental Mass Transfer Coefficients. Hundreds of papers have been published reporting mass transfer coefficients in packed columns.

For some simple systems which have been studied quite extensively, mass transfer data may be obtained directly from the literature (6). The situation with respect to the prediction of mass transfer coefficients for new systems is still poor. Despite the wealth of experimental and theoretical studies, no comprehensive theory has been developed, and most generalizations are based on empirical or semiempirical equations.

Liquid-Phase Transfer. It is difficult to measure transfer coefficients separately from the effective interfacial area; thus data is usually correlated in a lumped form, eg, as $k_L a$ or as H_L. These parameters are measured for the liquid film by absorption or desorption of sparingly soluble gases such as O_2 or CO_2 in water. The liquid film resistance is completely controlling in such cases, and $k_L a$ may be estimated as $K_{OL} a$ since $x_i \approx x^*$ (Fig. 17). This is a prerequisite because the interfacial concentrations would not be known otherwise and hence the driving force through the liquid film could not be evaluated.

The resulting correlations fall into several categories. Some are essentially empirical in nature. Examples include a classical correlation proposed by Sherwood and Holloway (113).

$$H_L = \frac{1}{\alpha}\left(\frac{L}{\mu}\right)^n \left(\frac{\mu_L}{\rho_L D_L}\right)^{0.5} \tag{83}$$

The values of α and n are given in Table 3; typical values for D_L can be found in Table 4. The exponent of 0.5 on the Schmidt number $(\mu_L/\rho_L D_L)$ supports the penetration theory. Further examples of empirical correlations provide partial experimental confirmation of equation 83 (3,114–118). The correlation reflecting what is probably the most comprehensive experimental basis, the Monsanto Model, also falls in this category (118,119). It is based on 545 observations from 13 different sources and may be summarized as

$$H_L = \phi C_{fl}\left(\frac{h}{3.05}\right)^{0.15} \mathrm{Sc}^{0.5}{}_L \tag{84}$$

The packing parameter $\phi(m)$ reflects the influence of the liquid flow rate as shown in Figure 18. C_{fl} reflects the influence of the gas flow rate, staying at

Table 3. **Values of Constants for Equation 83**

Packing	Size, cm	α^a	α^b	n
Raschig rings	0.95	3120	550	0.46
	1.3	1390	280	0.35
	2.5	430	100	0.22
	3.8	380	90	0.22
	5.1	340	80	0.22
Berl saddles	1.3	685	150	0.28
	2.5	780	170	0.28
	3.8	730	160	0.28

[a] Valid for units kg, s, m.
[b] Valid for units lb, h, ft.

Table 4. **Diffusion Coefficients for Dilute Solutions of Gases in Liquids at 20°C**

Gas	Liquid	D_L, $m^2/s \times 10^{-9}$
CO_2	water	1.78
Cl_2	water	1.61
H_2	water	5.22
HCl	water	0.61
H_2S	water	1.64
N_2	water	1.92
N_2O	water	1.75
NH_3	water	1.83
O_2	water	2.08
acetone	water	1.61
benzene	kerosene	1.41

unity <50% of the flooding rate but beginning to decrease above this point. At 75% of the flooding velocity, $C_{fl} = 0.6$. Sc_L is the Schmidt number of the liquid.

Other correlations based partially on theoretical considerations but made to fit existing data also exist (121–128). A number of researchers have also attempted to separate k_L from a by measuring the latter, sometimes in terms of the wetted area (56,129,130). Finally, a number of correlations for the mass transfer coefficient k_L itself exist (131,132). These are based on a more fundamental theory of mass transfer in packed columns (133–136). Although certain predictions were verified by experimental evidence, these models often cannot serve as design basis because the equations contain the interfacial area a as an independent variable. Only few correlations for the interfacial area in structured packing are available (122,124). Based on a mechanistic model for mass transfer, a way to estimate HETP values for structured packings in distillation columns has been proposed (137), yet there is a clear need for more experimental data in this area.

Gas-Phase Transfer. The height of a gas-phase mass transfer unit, or $k_G a$, is normally measured either by vaporization experiments of pure liquids, in which no liquid mass transfer resistance exists, or using extremely soluble gases. In the latter case, m is so small that the liquid-film resistance in equation 7 is negligible and the gas-film mass transfer coefficient can be observed as $k_G a \approx K_{OG} a$ and $y_i \approx y^*$. The experiments are difficult because they have to be carried out in very shallow beds. Otherwise, all of the highly soluble gas is absorbed and the driving force cannot be evaluated. The resulting end effects are probably the main reason for the substantial disagreement of the published data, which have been reported to vary some threefold for the same packing and flow rates (137). Furthermore, the effective interfacial areas seem to differ for absorption and vaporization (138). During the absorption experiments, the many stagnant or semistagnant pockets of liquid which exist in a packing tend to become saturated and thus ineffective. This is not the case in vaporization experiments where the total effective interfacial area consists of the surface area of moving liquid plus the semistagnant liquid pockets.

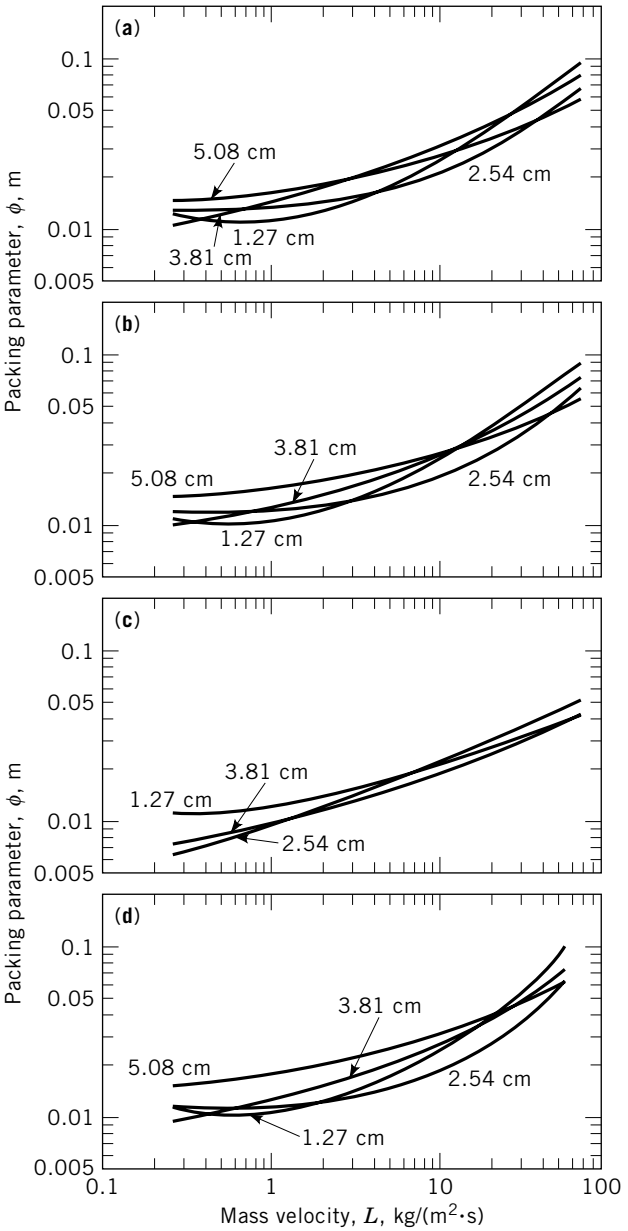

Fig. 18. Improved packing parameters ϕ for liquid mass transfer: (**a**) ceramic Raschig rings; (**b**) metal Raschig rings; (**c**) ceramic Berl saddles; (**d**) metal Pall rings (119). Reprinted with permission (120).

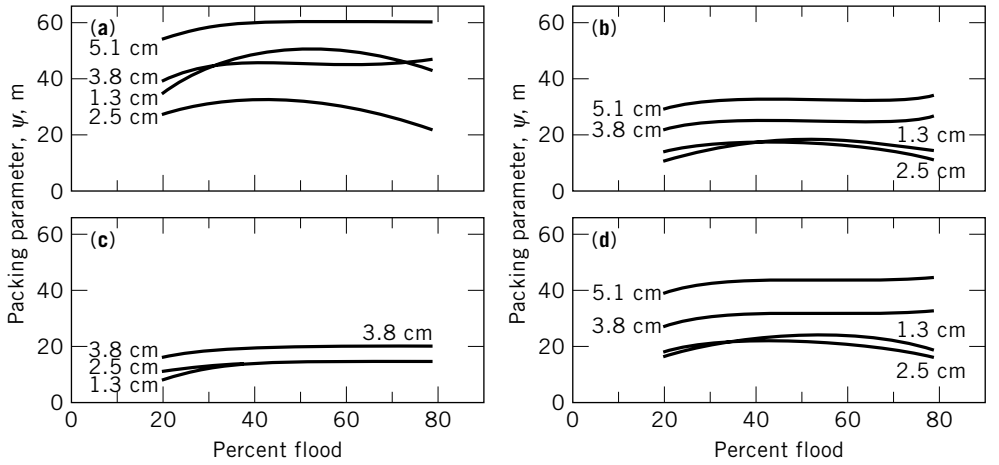

Fig. 19. Improved packing parameters ψ for gas mass transfer: (**a**) ceramic Raschig rings; (**b**) metal Rashig rings; (**c**) ceramic Berl saddles; (**d**) metal Pall rings (119). Reprinted with permission.

The correlation of H_G based on the most extensive experimental basis is again the Monsanto model (119):

$$H_G = \psi \frac{(3.28 d'_c)^m (h/3.05)^{1.3}}{(737 L f_\mu f_\rho f_\sigma)^n} Sc_G^{0.5} \tag{85}$$

where d'_c is the lesser of 0.61 or column diameter, m; $f_\mu = (\mu_L/\mu_w)^{0.16}$; $f_\rho = (\rho_L/\rho_w)^{-1.25}$; $f_\sigma = (\sigma_L/\sigma_w)^{-0.8}$; Sc_G = Schmidt number of the gas. The packing parameter ψ in m, depends on the gas flow rate as shown in Figure 19. Values of the diffusivity of various solutes in air and typical Schmidt numbers for use in equation 85 are found in Table 5. The exponents m and n adopt the values of 1.24 and 0.6, respectively, for rings as packing materials, and 1.11 and 0.5, for saddles.

Mass transfer coefficients in the gas phase for traditional (dumped) packings are often computed from the correlation of Onda, either in the original form (56) or in a more recent and improved form (55). Useful correlations for structured packings have been published by Bravo and co-workers (53) and Spiegel and Meier (139). Software packages implementing kinetic design methods typically offer a number of alternatives for mass transfer correlation (123).

Another type of experiment to measure k_G separately from other factors consists of saturating packings made from porous materials using a volatile liquid and subsequently drying it by passing a stream of inert gas through the packing (140–143). Since the surface of the packing is normally known in these experiments, k_G can be computed. Application of these kinds of data to gas absorption design is difficult, however, because of the different, unknown effective interfacial areas when two phases are flowing through the packing. A similar approach was used by evaporating naphthalene from a packing made

Table 5. **Values of the Diffusion Coefficient D_A and of $\mu_G/D_A\rho_G$ for Various Gases in Air at 0°C and at Atmospheric Pressure**[a]

Gas	CAS Registry Number	D_A, $m^2/s \times 10^{-5}$		μ_G
		Calculated	Experiment	$\rho_G D_A$
acetic acid	[64-19-7]		1.05	1.26
acetone	[67-64-1]	0.83		1.60
ammonia	[7664-41-7]	1.62	2.17	0.61
benzene	[71-43-2]	0.72	0.78	1.71
bromobenzene	[108-86-1]	0.67		1.71
butane	[106-97-8]	0.75		1.77
n-butyl alcohol	[71-36-3]		0.69	1.88
carbon dioxide	[124-38-9]	1.19	1.39	0.96
carbon disulfide	[75-15-0]		278.00	1.48
carbon tetrachloride	[56-23-5]	0.61		2.13
chlorine	[7782-50-5]	0.92		1.42
chlorobenzene	[108-90-7]	0.61		2.13
chloropicrin	[76-06-2]	0.61		2.13
2,2′-dichloroethyl sulfide (mustard gas)	[505-60-2]	0.56		2.44
ethane	[74-84-0]	1.08		1.22
ethyl acetate	[141-78-6]	0.67	0.72	1.84
ethyl alcohol	[64-17-5]	0.94	1.03	1.30
ethyl ether	[60-29-7]	0.69	0.78	1.70
ethylene dibromide	[106-93-4]	0.67		1.97
hydrogen	[1333-74-0]	5.61		0.22
methane	[74-82-8]	1.58		0.84
methyl acetate	[79-20-9]		0.94	1.57
methyl alcohol	[67-56-1]	1.22	1.33	1.00
naphthalene	[91-20-3]		0.50	2.57
nitrogen	[7727-37-9]	1.33		0.98
n-octane	[111-65-9]		0.50	2.57
oxygen	[7782-44-7]	1.64	1.78	0.74
pentane	[109-66-0]	0.67		1.97
phosgene	[75-44-5]	0.81		1.65
propane	[74-98-6]	0.89		1.51
n-propyl acetate	[109-60-4]	0.67	0.67	1.97
n-propyl alcohol	[71-23-8]	0.81	0.86	1.55
sulfur dioxide	[7446-09-5]	1.03		1.28
toluene	[108-88-3]	0.64	0.72	1.86
water	[7732-18-5]	1.89	2.19	0.60

[a] The value of μ_G/ρ_G is that for pure air, 1.33×10^{-5} m^2/s. Diffusion coefficients may be corrected for other conditions by assuming them proportional to $T^{2/3}$ and inversely proportional to P. The Schmidt numbers depend only weakly on temperature (139).

from this material (130,138). The mass transfer coefficient k_G measured in this manner was then combined with k_G a data (144) to determine the effective area, which was found to be fairly independent of gas rate up to the loading point. The data bank underlying the Monsanto Model and literature correlations for k_G and k_L (130,138) have also been used (145) to develop a new correlation for packed distillation columns.

Height Equivalent to a Theoretical Plate. Provided both the equilibrium and operating lines are straight, HETP values may be estimated by combining

the H_G and H_L values predicted by the above correlations and by translating the resulting H_{OG} into HETP by combining equations 56, 60, and 65 with equation 95, which is discussed under bubble tray absorption columns:

$$HETP = \frac{\ln(mG_M/L_M)}{(mG_M/L_M) - 1} H_{OG} \tag{86}$$

The HETP values obtained in this way have been compared to measured values in data banks (119) and statistical analysis reveals that the agreement is better when equations 84 and 85 are used to predict H_G and H_L than with the other models tested. Even so, a design at 95% confidence level would require a safety factor of 1.7 to account for scatter. The use of HETP in the special case of absorption with chemical reaction is discouraged, since the equilibrium line for many systems of chemical absorption is virtually horizontal. Therefore the absorption factor defined in the usual way $L_M/G_M m$ tends to infinity , the number of theoretical plates required apparently goes to zero and the height equivalent to a theoretical plate predicted by equation 86 tends to infinity. The more natural HTU/NTU approach is preferred (even for horizontal equilibrium line, the integral that defines the required NTU is well behaved).

5. Case Studies

In real-world situations one will sometimes be confronted simultaneously with several of the complications treated schematically above. Standard design proceedures may then yield little more than a first approximate idea of packing requirements and column operation. Even a trustwothy preliminary design should be based in such situations on a computer calculation of the concentration profiles. As an illustration of how the principles of mass transfer and packed column design discussed earlier may be used in computer models, we present in what follows two relatively complex real-world cases of gas absorption processes.

5.1. Absorption with Chemical Reactions. The number and variety of industrial applications of absorption with chemical reaction has grown significantly in the last decade, partly driven by environmental considerations and partly by the increased use of natural gas as an energy source. Some typical applications include the absorption of NO_x in aqueous solutions in the synthesis of nitric acid (68) or in caustic in the synthesis of sodium nitrite (69), selective and unselective absorption of H_2S from sour gas streams, possibly containing large amounts of CO_2 using amines, refinery sour water stripping operations, regenerative Wellman-Lord desulfurization of flue gases by means of sodium sulfites (70).

Such applications almost invariably involve a complex set of reactions, the chemical reaction kinetics and equilibrium data of which are not always available or reliably known. These difficulties represent a serious obstacle to the rigorous design of chemical absorbers. Consequently, designs are very often complemented by extensive laboratory and pilot plant tests. In spite of design uncertainties, the benefits to be gained from gas absorption with chemical reaction have not been overlooked by the chemical and petrochemical industries and new applications and processes appear continually (71).

The selective absorption of H_2S from CO_2-rich sour natural or process gases is a good illustration of the significant advances achieved in the field and motivated by the increased use of sour natural gases: up to approx. the early 1980s large amounts of sweet natural gases, containing little if any H_2S and CO_2 were readily available. Such gases could be treated with unselective solvents that absorbed both acid components. As production from sweet gas wells started to dwindle, other sour natural gas sources had to be tapped.

Treating such sour gases with a conventional amine (like monoethanolamine MEA) in order to reduce H_2S concentrations to an acceptable level would lead to the absorption of a very large fraction of the accompanying CO_2. The resulting absorption plant would then be unnecessarily overdesigned, both in the size of the equipment and in the energy requirements for amine regeneration. Through the use of amines such as methyl-diethanolamine (MDEA) or of the sterically hindered 2-amino-2-methyl-1-propanol (AMP) it is nowadays possible to meet H_2S specifications while co-absorbing a moderate amount of CO_2 thus greatly improving the economics of the process. Hindered amines are finding increased application in this area since it is generally believed that steric effects reduce the stability of the carbamates formed by the amine with CO_2. The carbamates readily undergo hydrolysis and release free amine that again reacts with CO_2 thus increasing the loading capacity of the amine. In addition, hindered amines demonstrate very good selectivity towards H_2S in the presence of CO_2. Consequently, hindered amines have found their way into commercial gas treating processes such as Flexsorb SE (72). However, even in well documented cases, like H_2S/CO_2 absorption with AMP (73,74) the chemical complication of the system can be appreciable. As an illustration of the type of calculations involved in gas absorption with subsequent chemical reaction in the liquid phase, we will consider the absorption of moderate amounts of carbon dioxide CO_2 and hydrogen sulphide H_2S (in a molar ratio of 3:1) from a low pressure fuel gas stream into a methyl-diethanolamine (MDEA) solution. This application is a good representative of a typical sweetening application for a semi-sour refinery fuel gas (71). Absorption will be carried out in a column packed with structured packing. At the relatively low specific liquid load required (15 m^3/m^2 h), there is no appreciable hydrodynamic gas-liquid interaction and liquid flow over the corrugated metal packing sheets is laminar to a very good approximation (see Refs. 54, 139 for a detailed description of the packing geometry). For the time being, we will assume that no appreciable heat effects need to be taken into account, ie, we will consider isothermal absorption only.

Mass transfer in the gas phase will be handled by means of mass transfer coefficients valid for structured packings (53,132,139). We will focus on a short section of packing between two bends. Additionally, we will assume the diffusive contribution to the flux in the direction of the liquid flow to be negligible with respect to convection, ie, the mechanism of transfer across the liquid film is diffusion, whereas along the film convection is the dominant mechanism.

The following table lists the chemical species present in the system:

species	H_2O	OH^-	H_3O^+	CO_2	HCO_3^-	CO_3^{2-}	H_2S	HS^-	S^{2-}	MDEA	$MDEA^+$
species label	1	2	3	4	5	6	7	8	9	10	11

The reactions to be considered are:

1. Water dissociation:

$$2\ H_2O \leftrightarrow H_3O^+ + OH^-$$

2. CO_2 first dissociation:

$$CO_2 + 2\ H_2O \leftrightarrow H_3O^+ + HCO_3^-$$

3. CO_2 second dissociation:

$$HCO_3^- + H_2O \leftrightarrow H_3O^+ + CO_3^{2-}$$

4. H_2S first dissociation:

$$H_2S + H_2O \leftrightarrow H_3O^+ + HS^-$$

5. H_2S second dissociation:

$$HS^- + H_2O \leftrightarrow H_3O^+ + S^{2-}$$

6. MDEA protonation:

$$H_3O^+ + MDEA \leftrightarrow MDEAH^+ + H_2O$$

Proper kinetics will be taken into account for all the previous reactions, i.e. we will not assume chemical equilibrium for any of these reactions. We have kept the previous set of chemical reactions as complete as possible for illustration purposes and because for a general system it is not always obvious a priori which, if any, of a set of reactions can be neglected or treated in simplified manner. For H_2S and CO_2 absorption in MDEA, it is usual to reduce the number of chemical reactions (and accompanying kinetic parameters) by neglecting the concentrations of S^{2-} and CO_3^{2-}. This would be reasonable in the present case because, for both gases, the second dissociation constant is at least a factor of 1000 smaller than the first one. A usual second assumption is to neglect OH^- and H^+ concentrations at all gas loadings (146) because both MDEA and acid gases are a weak base and weak acids in water, respectively.

Extensive transport, kinetic and thermodynamic data for this system are available in Refs. 146–153. The assumptions stated above of isothermal operation, liquid laminar flow, use of mass transfer coefficients for the gas phase and no axial dispersion due to diffusion allow us to write balance equations for all components in the liquid control volume defined in Figure 20. This figure represents the flow between two bends in a packing element. Upon reaching the next bend, the fluid is mixed and concentration gradients across the film

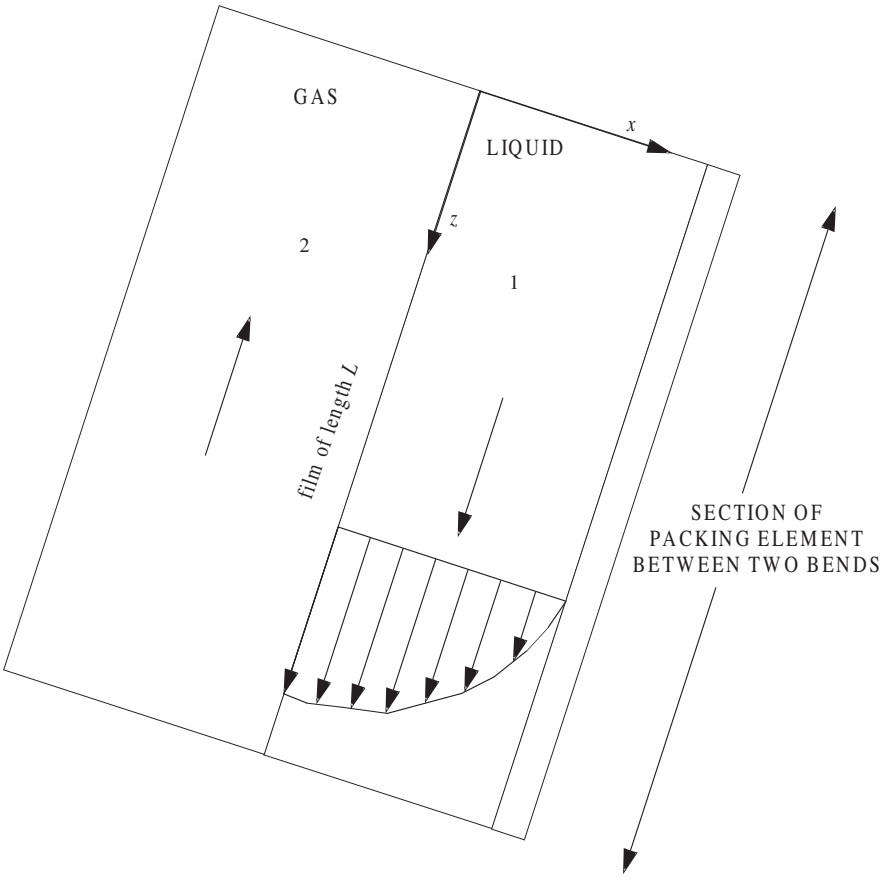

Fig. 20. Schematic of contercurrent absorption from a gas into a laminar film flowing along a structured packing.

equalized. A succession of such laminar flows followed by complete mixing is a widely accepted mechanism for liquid side mass transfer in structured packings (22,145). Mass transfer and complex chemical reaction in each of the laminar flow sections can therefore be treated naturally by means of the following scheme:

For each of the species, the following differential mole balance equation must hold in the liquid domain Ω_1:

$$-D_i \frac{\partial^2 c_1}{\partial x^2} + v_z \frac{\partial c_j}{\partial z} - \sum_j r_{ij} = 0 \qquad i = 1, 11 \quad j = 1, 6 \tag{87}$$

where $v_z = 3/2\,\bar{v}\,(x/\delta)^2$ is the velocity profile across the film, $\bar{v}$ is the average liquid velocity (proportional to the liquid throughput), δ is the film thickness and r_{ij} is the reaction velocity for species i in reaction j (here we follow the nomenclature and sign conventions of Ref. 154).

In the gas domain Ω_2, the following differential mode balance equations must hold for the two species undergoing transfer:

$$\frac{dp_{co_2}}{dz} = -\frac{Pk_{g,CO_2}}{G}\ (p_{CO_2} - H_{CO_2}c_{CO_2}) \tag{88}$$

$$\frac{dp_{H_2S}}{dz} = -\frac{Pk_{g,H_2S}}{G}\ (p_{H_2S} - H_{H_2S}c_{H_2S}) \tag{89}$$

where P is the total pressure in the column and G the gas load (moles per unit area per unit time).

In addition, for Eq. (87) the following boundary conditions must be imposed:

$$c_i(x,0) = 0 \qquad \text{for} \quad i = 4-9, 11$$

$$c_j(x,0) = c_i^0 \qquad \text{for} \quad i = 1, 2, 3, 10$$

which correspond to inlet of unloaded MDEA solution at the top. Boundary conditions for mass transfer across the film must also be imposed:

$$-D_i\ \frac{\partial c_j}{\partial x}\bigg|_{\substack{x=\delta \\ \forall z}} = 0 \qquad \text{for} \qquad i = 1, 2, 3, 5, 6, 8-11$$

$$-D_{CO_2}\ \frac{\partial c_{CO_2}}{\partial x}\bigg|_{\substack{x=\delta \\ \forall z}} = k_{g,CO_2}\ (p_{CO_2} - H_{CO_2}c_{CO_2}) \tag{90}$$

$$-D_{SH_2}\ \frac{\partial c_{SH_2}}{\partial x}\bigg|_{\substack{x=\delta \\ \forall z}} = k_{g,SH_2}(p_{SH_2} - H_{SH_2}c_{SH_2}) \tag{91}$$

And finally,

$$-D_i\ \frac{\partial c_i}{\partial x}\bigg|_{\substack{x=0 \\ \forall z}} = 0 \qquad \text{for} \quad i = 1-11$$

at the surface of the packing (packing impenetrable to mass transfer).

For Eqs. (88) and (89) the following gas inlet boundary conditions must be imposed:

$$p_{CO_2}(\mathrm{L}) = p^0_{CO_2} \qquad \text{and} \quad p_{H_2S}(\mathrm{L}) = p^0_{H_2S}$$

where $p^0_{CO_2}$ and $p^0_{H_2S}$ are the partial pressures of the sour components at the gas inlet ($z = L$).

The solution sought are thus the concentrations of all species throughout the liquid domain and the partial pressures of the sour components in the gas domain.

Although these equations are quite simple to write formally, they contain terms such as Henry's constants, which are reather tedious to compute, since

they are a complicated function of composition, temperature and pressure (eg, in the present example, the Clegg-Pitzer equation of state was used to describe sour gas solubility).

It is important to keep in mind that this approach leads to a rather large system of mixed partial (for the liquid phase, where reaction and diffusion take place) and ordinary (for the gas phase where the mass transfer formalism is applied) differential equations. The equations in the liquid domain are strongly coupled through the kinetic terms r_{ij}. The solution of the system is further complicated by numerical difficulties which appear if variables are not scaled properly. Marching or multiple shooting methods (155) are not very successful in this type of calculations. Nevertheless, the geometry of the example is simple enough so that rather straightforward Finite Differences (FD) methods can be used. In a general case with a more complex geometry, however, a Finite Element (FE) approach is mandatory. Figure 21 shows the concentration profiles of the sour components in the film at four different positions along the packing computed using a FE method to solve the set of Eqs. 87–89 with their boundary conditions.

Doubly ionized species are present in very low concentrations, as expected. Hence the usual assumption of neglecting them in practical calculations. Additionally, the selective absorption of CO_2 over H_2S by the amine is also evident (notice the differences in scales in the ordinates of both plots). Although the amount of CO_2 in the gas feed is three times larger than that of H_2S, the selectivity of MDEA results in a enhanced absorption of hydrogen sulfide, as is shown by the concentration of HS^- being approximately ten times higher than that of bicarbonate at all locations within the film. Higher point selectivities can be reached in practice by careful selection of solvent, column internals and operating conditions. For column and internal optimization, the problem has to be solved repeatedly, and especialized software packages (see below under Design of Nonisothermal Scrubbers with Chemical Reactions) are a requirement.

Although computationally expensive, the advantage of this approach is that it is rate-based and yields full information on concentration profiles for all components. In addition, concentration dependent diffusivities can be incorporated in the calculation easily.

5.2. Nonisothermal Scrubbers with Chemical Reactions. Amine scrubbers may serve as an example for gas absorption processes involving both chemical reactions and heat effects. In addition to detailed knowledge of transport, equilibrium and reaction kinetics, the design of amine scrubbers has to take into account large absorption heat effects (see section on Nonisothermal Gas Absorption above). Complex design cases like gas sweetening require an understanding of both phase behavior coupled with chemical equilibrium and mass transfer accompanied by chemical reactions (75,76). The complexity of the design makes it necessary to resort to highly specialized software packages (AMSIM from DBR Software Inc, Hysys from Hyprotech/AEA Technology plc, PROSIM and TSWEET from Bryan Research and Engineering, Inc, etc) or to special packages within general purpose flowsheet simulators. Most flowsheet simulators contain nowadays optional data packages in which full kinetic and equilibrium data are contained (ASPEN PLUS from Aspen Technologies, PRO/II from SimSci, Design II from WinSim, Inc., etc).

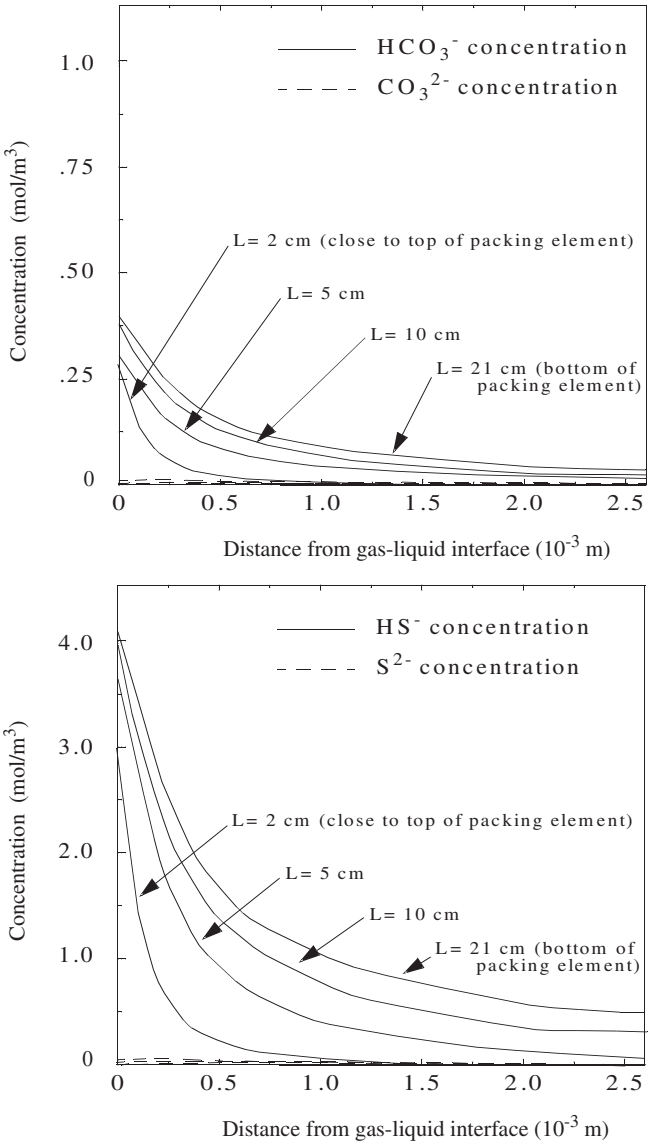

Fig. 21. Concentration profiles across liquid film for sour components. Isothermal case.

These special-purpose programs or packages typically utilize a modified form of the Murphree Stage Efficiency model to calculate the stage efficiency at each stage in the column, rather than using an ideal stage approach for the entire column. This allows the calculation of individual component stage efficiencies as a function of pressure, temperature, phase compositions as well as kinetic and mass transfer parameters. Alternatively, they use more advanced and rigorous approaches, based on nonequilibrium models and even including the

possibility of dynamic modeling (51,77). It must be said that these advanced design techniques are very demanding in terms of computation and its industrial application is therefore not very widespread yet. Nevertheless given the rapid growth of performance/cost ratio for computing hardware, they will very probably see increased usage in coming years. The sophistication of numerical design procedures has reached a point where the current limiting factor in practice, from the user's point of view is the availability of reliable thermodynamic, chemical and transport properties.

In order to illustrate a rigorous calculation procedure for chemical reaction with heat effects, we will again consider the sour gas sweetening example already presented but we will now remove the assumption of isothermal operation. This situation arises when the reaction enthalpies and the rate of absorption of sour gases (i.e. the heat release rate) are sufficiently high. Assuming the reaction heat to remain entirely in the liquid, the system of equations (87–89 plus boundary conditions) are still valid if we now consider temperature dependent physical properties (reaction rates, specific heats, diffusivities, etc).

In addition, that system must be augmented by an energy balance equation with takes the form:

$$-k_{\text{sol}} \frac{\partial^2 T}{\partial x^2} + v_z \rho C_p \frac{\partial T}{\partial z} - \sum_j r_{ij}(T) \Delta H_{\text{R}_{ij}}(T) = 0 \qquad j = 1, 6$$

in which k_{sol}, ρ, and C_{p} are the thermal conductivity, the density of the solution and the specific heat of the solution (themselves weak functions of composition and temperature) and $\Delta H_{\text{R}_{ij}}(T)$ is the molar enthalpy of reaction number j referred to component i. Component i is the component to which chemical reaction rates and enthalpy of reaction are referred (154). Unlike the other thermophysical properties the term r_{ij} is very strongly temperature dependent (usually an Arrhenius dependence).

Under the assumption of no heat transfer between gas and liquid, the proper boundary conditions for the liquid temperature field are

$$\left.\frac{\partial T}{\partial x}\right|_{\substack{x=0 \\ \forall z}} = 0$$

at the surface of the packing (by symmetry, since both sides of the packing are covered by liquid),

$$\left.\frac{\partial T}{\partial x}\right|_{\substack{x=\delta \\ \forall z}} = 0$$

at the gas–liquid interphase and

$$T(x, 0) = T_0$$

at the inlet, where T_0 is the known inlet temperature of the liquid. The augmented system of equations necessitates numerical solution in order to obtain the concentration and temperature fields. Figure 22 shows the effect that taking

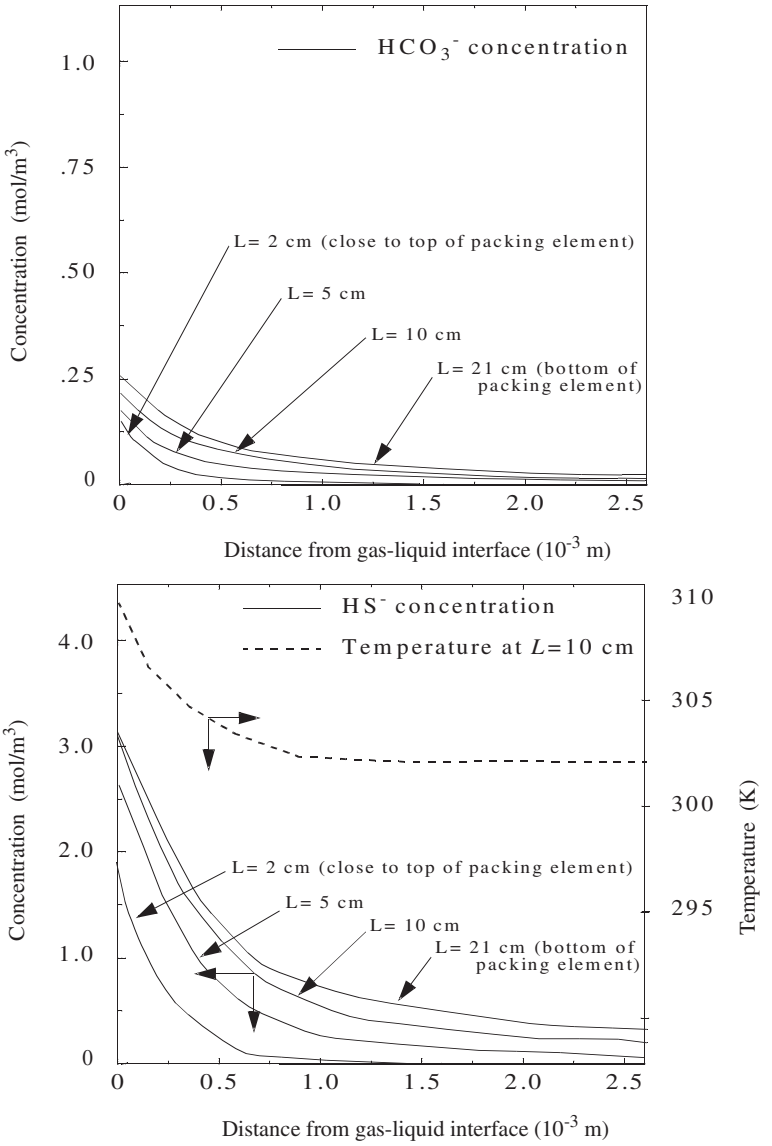

Fig. 22. Concentration profiles a cross liquid film for sour components. Nonisothermal case.

the heats of reaction into account has on the concentration profiles for the species associated with sour components:

Since the formation of both bicarbonate and hydrosulfide are both exothermic, temperature increases throughout the liquid film, but most appreciably close to the interphase. Sour component solubilities in this region drop correspondingly, leading to a reduction in the amounts absorbed. The overall rate of absorption drops by 28%. Selectivity, however, remains approximately the same as in the isothermal case.

The results presented in Figure 21 were obtained under the assumption that no heat transfer takes place by conduction or convection between both phases. This approximation can be removed, if interphase heat transfer coefficients are known, by adding another heat balance (ordinary differential) equation for the gas. In industrial practice it is however quite usual to work under the adiabatic assumption for the liquid phase in the cases where the gas is cooler than the liquid or where solvent evaporation takes place. The assumption of adiabatic liquid phase eliminates the cooling effect of the gas and thus leads to higher liquid temperatures, less effective absorption and to correspondingly more conservative design of contacting equipment.

A similar situation is often encountered for heat effects due to evaporation or condensation of solvent: the latent heat can be a cause of cooling or heating of the liquid phase that can be incorporated in the equations above adding the term for release of latent heat in the energy balance equation. Standard commercial software is generally able to take this solvent effect into account. But preliminary designs are often performed excluding latent heat terms in the cases where this exclusion leads to more conservative and, hence, safer design.

However, in those cases where the gas stream enters the column at a higher temperature than the liquid, taking proper account of heat transfer between phases is mandatory.

In all cases, during the final design stage, where tighter designs are required, the full mass and energy balance equations must be considered.

It is important to emphasize that including heat effects in the formulation increases the number of equations by one (or by one partial and one ordinary differential equation if heat transfer between gas and liquid is to be considered as well), ie, in a multicomponent system, it represents only a moderate increase in computation. Furthermore, experience shows that the heat balance equation itself is well behaved and seldom causes additional numerical problems.

Complex as the situation is in sour gas treating, it is not nearly as involved as in other cases, like sour water strippers (78) or flue gas treating (79) where the product stream to be treated is a very complex reacting mixture of a large number of species of not always exactly known composition. As an example, a widely used flue gas treating modeling package involves a set of 36 chemical reactions in which 26 nonionic species participate. Additional ionic species are produced from these aqueous phase ionic reactions so that the system actually contains 22 additional components (80).

By now a significant body of specialized literature dealing with the general subject of absorption with chemical reaction is available (51,71,81–84). Nevertheless, it is probable that an even larger amount of information, mainly data on thermophysical and equilibrium properties and column internals, is kept as proprietary by the companies which have developed specific processes. As is obvious from the preceding example, the rigorous design of chemical absorption columns, whether isothermal or not, requires considerable computational effort.

6. Capacity Limitations of Packed Absorption Columns

Thus far the discussion has been confined to factors affecting the tower height required to perform a specific absorption job. The necessary tower diameter, on

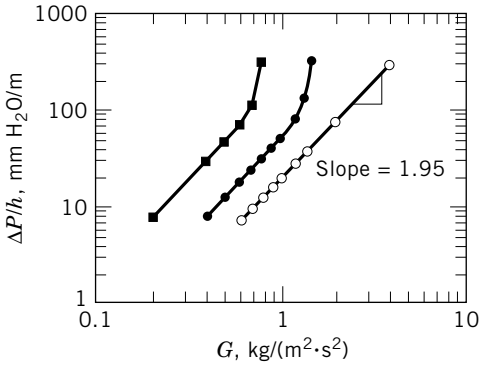

Fig. 23. Schematic representation of typical pressure drop as a function of superficial gas velocity, expressed in terms of $G = \rho_G u_G$, in packed columns. ○, Dry packing; ●, low liquid flow rate; ■, higher liquid flow rate. The points do not correspond to actual experimental data, but represent examples.

the other hand, depends primarily on the total amount of gas and liquid that must be handled. At a given set of flow rates, the diameter of the packing can only be decreased at the expense of a large pressure drop, which in turn generates higher operating costs because more power is needed to blow the gas through the packing. The reason for this is the fact that handling a given total gas flow rate in a smaller tower diameter increases the superficial velocity at which the gas has to be pushed through the packing.

The relationship between the pressure drop per unit of packed height and the superficial gas velocity given in terms of the gas flow rate is shown schematically in Figure 23. In a dry packing, ΔP increases almost as the square of the gas velocity, which is in accord with the turbulent nature of the flow. At low liquid flow rates, the curves are somewhat shifted upwards because the presence of liquid films restricts the free section available for gas flow and thus increases the linear gas velocity somewhat. Because the liquid hold-up remains independent of G, the slope of the curve in this log–log plot remains close to 2. At higher pressure drops, however, the upflowing gas impairs the downflow of liquid and excess liquid starts to accumulate in the packing, thereby increasing the hold-up. In this operating region, called the loading zone, the increasing liquid hold-up restricts the free section available for the gas flow further as G becomes larger. Hence the linear gas velocities increase faster than G and the power dependence of ΔP on G starts to rise >2. The G value at which the curve begins to deviate from the straight line has been defined as the loading point.

If the tower diameter is made too small for a given total gas flow rate, that is, if u_G and G are increased above a certain critical value, ΔP becomes so great that the liquid cannot flow downward anymore over the packing, but is blown out the top of the packing. The vertical asymptotes on Figure 23 indicate the gas rates at which this condition, called flooding, occurs. This gas flow rate at flooding, G_F, determines the theoretical minimum diameter at which the tower is operable, and knowledge of it is therefore very important. Flooding rates have been correlated (156–158).

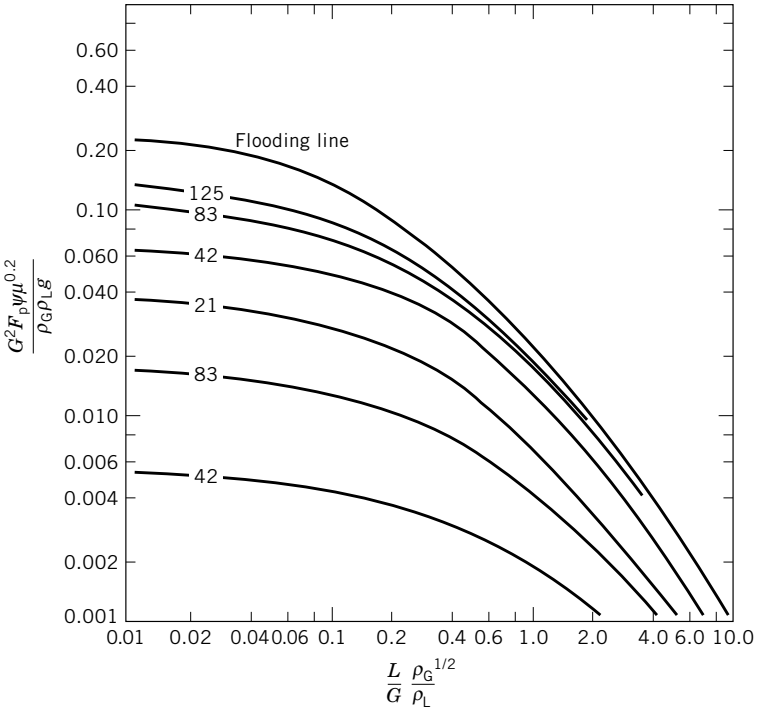

Fig. 24. Pressure drop and flooding correlation for various random packings (159). $\psi = \rho_{H_2O}/\rho_L$, g (standard acceleration of free fall) $= 9.81 m/s^2$, μ = liquid viscosity in mPa · s; s; numbers on lines represent pressure drop, mm H_2O/m of packed height; to convert to in. H_2O/ft multiply by 0.012. Packing factors for various packings have been published (160) and are reproduced in part in Table 6.

Table 6. **Characteristics of Dumped Tower Packings**[a]

Packing type	Nominal size, mm	Surface area, m^2/m^3	Packing factor, F_P, m^{-1}
Raschig rings, ceramic	6	710	5250
	13	370	2000
	25	190	510
	50	92	215
Raschig rings, steel	25	185	450
	50	95	187
Berl saddles, ceramic	6	900	2950
	13	465	790
	25	250	360
	50	105	150
Pall rings, metal	25	205	157
	50	115	66
Pall rings, polypropylene	25	205	170
	50	100	82

[a] Ref. 160.

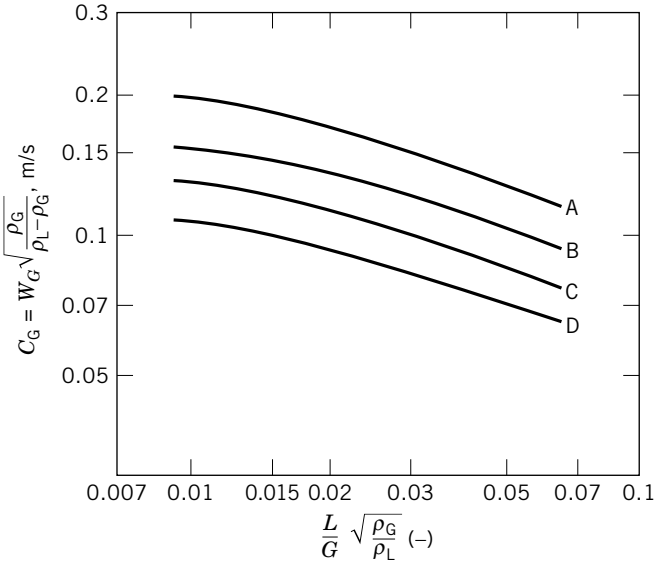

Fig. 25. Souders load diagram for capacity limit determination for four structured packings of the Sulzer-Mellapak type. The solid lines represent the capacity limits of the respective packings as defined by a pressure drop of 1.2 kPa/m: A, 125 *Y*; B, 250 *Y*; C, 350 *Y*; D, 500 *Y*. Flooding rates are ~5% higher. Reprinted with permission (139).

Both the pressure drop per unit length of packed tower and the gas flooding rate have been correlated for random packings as shown in Figure 24 (159). Such correlations enable predicting the gas flow rate G that will flood the packing at a given L/G ratio. In practice, the tower has to be operated at flow rates considerably less than the flooding rates for safety reasons. It is generally accepted that 50–80% of the flooding flow rates can be permitted. The curves plotted on Figure 24 thus also enable prediction of the pressure drop at any chosen operating value of G. The diameter of the column must then be evaluated by comparing this value to the total quantity of gas that the tower is supposed to handle. The correlation shown in Figure 24 can be applied to predict the hydraulic performance of many different packings owing to an adjustable parameter known as the packing factor F_P. Values for F_P have been compiled (160); a few examples are listed in Table 6. Similar flooding rate correlations are available for arranged packings. Figure 25 reports results for four examples of Mellapak types (139). Comparison of Figures 25 and 24 reveals higher capacity limits in structured than in many of the dumped packings. At similar loads, structured packings tend generally to give rise to less pressure drop.

7. Bubble Tray Absorption Columns

7.1. General Design Procedure. Bubble tray absorbers may be designed graphically based on a so-called McCabe-Thiele diagram. An operating line and an equilibrium line are plotted in y-x, Y'-X', or Y^0-X^0 coordinates using

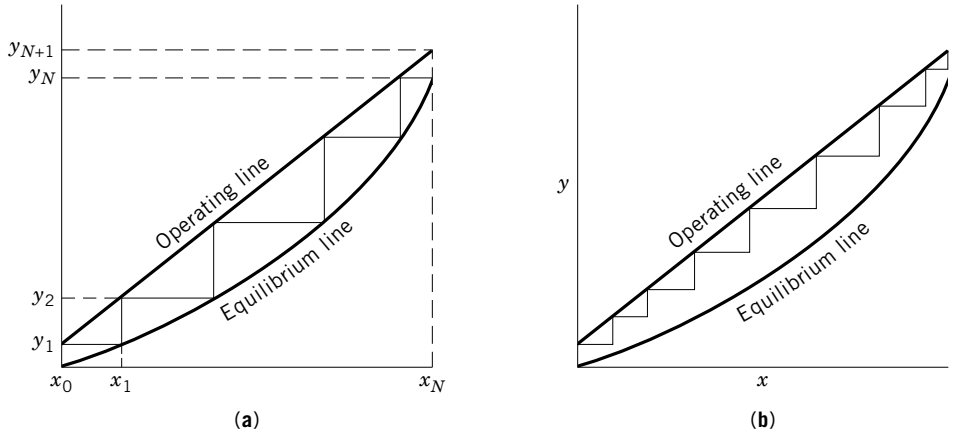

Fig. 26. McCabe-Thiele diagram. (**a**) Number of theoretical plates, 5; (**b**) number of actual plates, 8.

the principles for packed adsorbers outlined above (see Fig. 26). The minimum number of plates required for a specified recovery may be computed by assuming that equilibrium is reached between the two phases on each bubble tray. Thus the gas and the liquid leaving a tray are at equilibrium and a hypothetical tray capable of equilibrating the phase streams is termed a theoretical plate. Starting the calculation at the bottom of the tower, where the concentrations are y_{N+1} and x_N (see Fig. 27), the concentration leaving the lowest theoretical plate y_N may be found on the design diagram (Fig. 26**a**) by moving from the operating line vertically to the equilibrium line, because y_N is at equilibrium with x_N. Since the concentrations between two plates are always related by the operating line, x_{N-1} may be found from y_N by moving horizontally to the operating line. By repeating this sequence of steps until the desired residual gas concentration y_1 is reached, the number of theoretical plates can be counted.

The required number of actual plates, N_P, is larger than the number of theoretical plates, N_{TP}, because it would take an infinite contacting time at each stage to establish equilibrium. The ratio N_{TP}: N_P is called the overall column efficiency. This parameter is difficult to predict from theoretical considerations, however, or to correct for new systems and operating conditions. It is therefore customary to characterize the single plate by the so-called Murphree vapor plate efficiency, E_{MV} (161):

$$E_{MV} \equiv \frac{y_n - y_{n+1}}{y_n^* - y_{n+1}} \tag{92}$$

which indicates the fractional approach to equilibrium achieved by the plate. An efficiency of 80% means that the reduction in solute gas concentration effected by the plate is 80% of the reduction obtained from a theoretical plate. Corresponding actual plates may therefore be stepped off by moving from the operating line vertically only 80% of the distance between operating and equilibrium line (Fig. 26**b**). In some special cases having negligible resistance in the gas phase, E_{MV} values may become unreasonably small. It is then more logical to define a

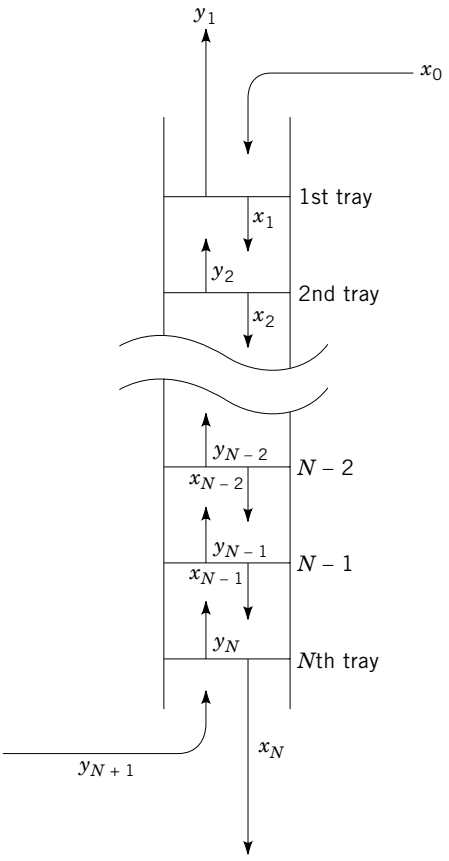

Fig. 27. Numbering plates and concentrations in a bubble tray column.

Murphree liquid plate efficiency, E_{ML}, simply by reversing the role of liquid and gas and by focusing on the change in liquid composition across the plate with respect to an equilibrium given by the leaving vapor.

7.2. Simplified Design Procedure for Linear Equilibrium and Operating Lines. A straight operating line occurs when the concentrations are low such that L_M and G_M remain essentially constant. (The material balance is obtained from eq. 44). In cases where the equilibrium K value does not depend too much on concentration, the use of absorption and stripping factors (162–164) allows rapid calculations for absorption design. One of the simplifying assumptions made in the development of this so-called Kremser-Brown method involves the use of the absorption factor A. The following algebraic expression describes the liquid and vapor flows from the plate (165):

$$A_n = \frac{L_n}{K_n G_n} \quad \text{or} \quad A_{av} = \frac{L_{av}}{K_{av} G_{av}} \tag{93}$$

where A_n is the absorption factor for each plate n and L_n and G_n are the liquid and vapor flows from the plate. The fractional absorption of any component by an

absorber of N plates is expressed in a form similar to the Kremser equation (163,164,166),

$$\frac{Y_{N+1} - Y_1}{Y_{N+1} - K_{x_0}} = \frac{A^{N+1} - A}{A^{N+1} - 1} \tag{94}$$

where Y_{N+1} = moles of absorbed component entering the column per mole of entering vapor and Y_1 = mole of absorbed component leaving the column per mol of entering vapor. The calculation of plate efficiency (163) is quite sensitive to the choice of equilibrium constants (4,167).

For linear equilibrium and operating lines, an explicit expression for the number of theoretical plates required for reducing the solute mole fraction from y_{N+1} to $y_1$has been derived (86):

$$N_{\mathrm{TP}} = \frac{\ln\left[\left(1 - \frac{mG_M}{L_M}\right)\left(\frac{y_{N+1} - mx_0}{y_1 - mx_0}\right) + \frac{mG_M}{L_M}\right]}{\ln\frac{L_M}{mG_M}} \tag{95}$$

This is the one case where the overall column efficiency can be related analytically to the Murphree plate efficiency, so that the actual number of plates is calculable by dividing the number of theoretical plates through equation 96:

$$\frac{N_{\mathrm{TP}}}{N_{\mathrm{P}}} = \frac{\ln\left[1 + E_{\mathrm{MV}}\left(\frac{mG_M}{L_M} - 1\right)\right]}{\ln\frac{mG_M}{L_M}} \tag{96}$$

7.3. Nonisothermal Gas Absorption. The computation of nonisothermal gas absorption processes is difficult because of all the interactions involved as described for packed columns. An very large number of plate calculations is normally required to establish the correct concentration and temperature profiles through the tower. Suitable algorithms have been developed (90,168) and nonisothermal gas absorption in plate columns has been studied experimentally and the measured profiles compared to the calculated results (91,169). Figure 28 shows a typical liquid temperature profile observed in an adiabatic bubble plate absorber (170). The close agreement between the calculated and observed profiles was obtained without adjusting parameters. The plate efficiencies required for the calculations were measured independently on a single exact copy of the bubble cap plates installed in the five-tray absorber.

A general, approximate, short-cut design procedure for adiabatic bubble tray absorbers has not been developed, although work has been done in the field of nonisothermal and multicomponent hydrocarbon absorbers. An analytical expression has been developed which will predict the recovery of each component provided the stripping factor, ie, the group mG_M/L_M, is known for each component on each tray of the column (165). This requires knowledge of the temperature and total flow (G_M and L_M) profiles through the tower. There are many suggestions about how to estimate these profiles (165,166,171).

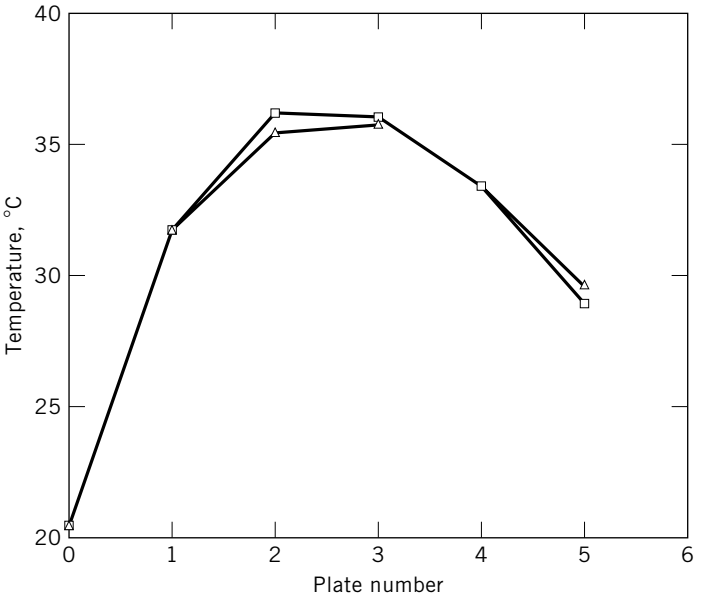

Fig. 28. Computed and experimental liquid temperature profiles in an ammonia absorber with five bubble cap trays (170). Water was used as a solvent. y_{N+1}=0.123; $y_1 = 0.0242$; $L'_M/G'_M = 1.757$; △ measured; □, calculated.

7.4. Plate Efficiency Estimation

Rate of Mass Transfer in Bubble Trays. The Murphree vapor efficiency, much like the height of a transfer unit in packed absorbers, characterizes the rate of mass transfer in the equipment. The value of the efficiency depends on a large number of parameters not normally known, and its prediction is therefore difficult and involved. Correlations have led to widely used empirical relationships, which can be used for rough estimates (172,173). The classical approach for tray efficiency estimation, however, remains the old Bubble Tray Design Manual (174), summarizing intensive research on this topic.

In large plates 0.6 m or more in diameter, the efficiency of the tray as a whole may differ from the efficiency observed at some particular point of the tray because the liquid is not uniformly mixed in the direction of the flow on the whole tray. The point value of the efficiency called E_{OG} is thus more closely related to interphase diffusion than E_{MV}. As the gas passes upward through the liquid covering a small area of the plate, mass transfer from gas to liquid occurs in a manner similar to a packed tower of height h_B, the depth of the bubbling area. Under the assumption that the liquid is completely mixed in the vertical direction, and that the gas travels through that minicolumn in a plug-flow-like fashion, the number of transfer units of the bubbling area may be calculated in terms of the gas concentrations above and below the area under consideration by applying the definition of N_{OG}, equation 64. This equation may be integrated by taking y^* as constant and equal to y_n^* because of the well-mixed nature of the liquid phase. By comparing the result with the definition of the plate efficiency,

equation 92, formulated for a single point on the plate, the following relationship between the point efficiency and the number of transfer units arises:

$$E_{OG} = 1 - e^{-N_{OG}} \tag{97}$$

If resistance to transfer is present in both phase, N_{OG} may be expressed as an addition of resistances using equations 63, 56, 50, 53:

$$\frac{1}{N_{OG}} = \frac{1}{N_G} + \frac{mG_M}{L_M}\,\frac{1}{N_L} \tag{98}$$

Hence, the point efficiency E_{OG} may be computed if both N_G and N_L in the bubbling area are known. These parameters are determined by the prevailing transfer coefficients, the interfacial area, and by h_B: $N_G = k_G a P h_B / G_M$ and $N_L = k_L a \rho h_B / L_M$.

To estimate the number of transfer units for design, the following empirical correlations which were derived from efficiency measurements employing a variety of trays and operating conditions under the aforementioned assumptions are recommended (174):

$$N_G = (0.776 + 4.63h_w - 0.238F + 0.0712L')\mathrm{Sc}^{-0.5} \tag{99}$$

where h_w is the weir height in m; $F = \rho_G(u_G)^{1/2}$ in m/s $[(\mathrm{kg/m^3})^{1/2}]$; L' is the liquid flow rate per average width of stream in $\mathrm{m^3/(s.m)}$; and

$$N_L = 3050\sqrt{D_L}\,(68h_w + 1)t_L \tag{100}$$

where $t_L = h_L z_L / L'$ is the liquid residence time in s. The recommended correlation for h_L is

$$h_L = 0.0419 + 0.19h_w - 0.0135F + 2.46L' \tag{101}$$

Effect of Different Degrees of Mixing. Once E_{OG} is evaluated on the basis of N_G and N_L using equation 83, it has to be translated into E_{MV} by considering the degree of mixing on the tray. It is obvious that for a small plate with completely backmixed liquid,

$$E_{MV} = E_{OG} \tag{102}$$

If, on the other hand, the liquid flows in a plug-flow-like manner over the tray, but the vapor may be assumed to mix between the trays so that it enters each tray in uniform composition, the result may be calculated according to (175).

$$E_{MV} = \frac{L_M}{mG_M}\left[e^{(mG_M/L_M)E_{OG}} - 1\right] \tag{103}$$

In the case of unmixed vapors between the plates, the equations, being implicit in E_{MV}, have also been solved numerically (175). The results depend on the

arrangement of the downcomers and are not too different numerically from equation 103. In reality, however, the liquid is neither completely backmixed nor can the tray be considered as a plug-flow device.

Many theories have been put forth to handle partial liquid backmixing on plates. Early calculations (139,176,177) used the so-called tanks-in-series model. Recycle models have been derived by assuming partial or complete backmixing of the liquid, or the vapor, or both (178–180). The suggested procedure (174) is based on the eddy diffusion model when the parameter characterizing the degree of liquid backmixing is the dimensionless group known as the Peclet number:

$$\mathrm{Pe} = \frac{z_{\mathrm{L}}^2}{D_{\mathrm{E}} t_{\mathrm{L}}} \tag{104}$$

The eddy dispersion coefficient D_{E} has been measured and correlated empirically as

$$\sqrt{D_{\mathrm{E}}} = 0.00378 + 0.0179 u_{\mathrm{g}} + 3.69 L' + 0.18 h_{\mathrm{w}} \tag{105}$$

The nomenclature is the same as that used in equation 99 and 100.

The relationship between E_{MV}, E_{OG}, and Pe has been calculated according to the recommended formulas (173) and presented in tabular form (4). A plot of this data is shown in Figure 29. Complete backmixing is characterized by $\mathrm{Pe} = 0$ ($D_{\mathrm{E}} = \infty$), where $E_{\mathrm{MV}} = E_{\mathrm{OG}}$. In larger columns, in which the liquid is not completely mixed horizontally, E_{MV} can be seen from Figure 29 to become larger than the point efficiency and may thus even exceed 100% (181). Entrainment, as well as by-passing, are always detrimental to the plate efficiency. Analytical expressions to correct for entrainment and by-passing have been developed (182,183).

7.5. Capacity Limitations. The fluid flow capacity of a bubble tray may be limited by any of three principal factors.

1. Flooding, often the most restrictive of the limitations, occurs when the clear liquid height in the downcomer, H_{dc}, exceeds a certain fraction of the tray spacing. During operation, the liquid level in the downcomer builds up as a result of the head necessary to overcome the various resistances to liquid flow, including the friction in the downcomer itself and the hydraulic gradient across the plate. A significant portion in the liquid backup is caused by the need for the liquid to overcome the difference in pressure between the inside and the outside of the downcomer, which in turn is caused by the pressure drop of the vapors through the next higher plate. If the diameter of the column is made too small for a given flow, the vapor pressure drop and thus the liquid backup in the downcomers will increase to the point where some liquid spills onto the next higher tray, and flooding sets in. In principle, the condition may be corrected by increasing the diameter or the tray spacing. A conservative design requires a clear liquid head in the downcomer of no more than half the tray spacing to allow for froth entrapped in the downcomer. The maximum allowable superficial velocity based on the column cross section u_{G} may be roughly estimated

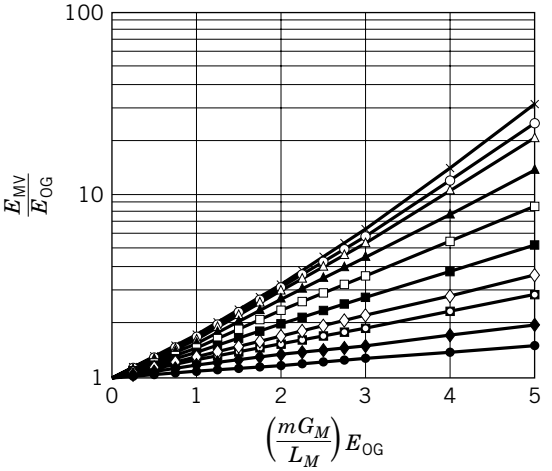

Fig. 29. Relationship between E_{OG} and E_{MV} at different degrees of liquid backmixing (4). Curves represent different Peclet numbers. From top to bottom Pe = ∞, +; Pe = 100, ○; Pe = 50, △; Pe = 20, ▲; Pe = 10, □; Pe = 5, ■; Pe = 3, ◇; Pe = 2, ■; Pe = 1, ◆; Pe = 0.5, ●.

for different tray spacings (6,184,185). A more reliable design would consider each pressure drop contributing to H_{dc} separately.

2. Entrainment occurs when spray or froth formed on one tray enters the gas passages in the tray above. In moderate amounts, entrainment will impair the countercurrent action and hence drastically decrease the efficiency. If it happens in excessive amounts, the condition is called priming and will eventually flood the downcomers.
3. At high liquid flow, the hydraulic gradient may become so large that the caps near the liquid feed point will stop bubbling, and the efficiency will suffer.

8. Nomenclature

Symbol	Definition	Units
A	L_M/mG_M, absorption factor	
a	effective interfacial area per packed volume	m^2/m^3
c_{Ai}	concentration of solute at interface	mol/m^3 or mol/L
C_P	specific heat of gas mixture	kJ/(mol·K)
C_q	specific heat of liquid mixture	kJ/(mol·K)
D_{ax}	axial dispersion coefficient	m^2/s
D_{AB}	diffusion coefficient of A in B	m^2/s
D_{Aj}	binary diffusion coefficient of A in the jth species other than A	m^2/s
$D_{A_{eff}}$	effective diffusion coefficient of A in a mixture, see Eq. 34	m^2/s
D_E	eddy dispersion (or diffusion) coefficient on a tray	m^2/s
D_L	liquid diffusion coefficient	m^2/s
E_{MV}	Murphree vapor plate efficiency, see equation 96	

Symbol	Definition	Units
E_{OG}	point value of plate efficiency	
F	$\mu_G\sqrt{\rho_G}$, F-factor for bubble tray gas load	$kg^{1/2}/(m^{1/2}\cdot s)$
g_j	moles of component j	mol
G_M	gas flow rate	$kmol/(m^2\cdot s)$
G'_M	flow rate of inert gas	$kmol/(m^2\cdot s)$
$G^0{}_M$	generalized molar gas flow rate, see equation 73	
H	Henry's constant	Pa
HETP	height equivalent to a theoretical plate	m
H_G	height of a gas-phase transfer unit, see equation 51	m
H_L	height of a liquid-phase transfer unit, see equation 54	m
H_{OG}	overall gas-phase height of a transfer unit, see equation 57	m
H_{OS}	integral heat of solution for the solute	kJ/mol
H_v	latent heat of pure solvent	kJ/mol
h	total height of packing	m
h_L	clear height of liquid on a tray	m
h_w	weir height	m
h_B	height of bubble layer on a tray	m
J_A	flux of component A due to diffusion	$mol/(m^2\cdot s)$
K	partition coefficient for gas–liquid equilibrium	
K_l	constant in bond stretching potential	$J/kmol\cdot m^2$
K_{OG}	overall gas-phase mass transfer coefficient	$mol/(s\cdot m^2\cdot Pa)$
K_θ	constant in bond bending potential	$J/kmol\cdot rad^2$
k_G	gas-phase mass transfer coefficient	$mol/(s\cdot m^2\cdot Pa)$
k_L	liquid-phase mass transfer coefficient	m/s
k_{sol}	thermal conductivity of the solution	$J/m\cdot K\cdot s$
$k^r{}_L$	mass transfer coefficient including effect of chemical reaction	m/s
k^0	mass transfer coefficient for equimolar counterdiffusion	m/s
k'	mass transfer coefficient for unidirectional molecular diffusion through a stagnant gas	m/s
k	mass transfer coefficient for general multicomponent diffusion situation	m/s
k_{Aj}	binary mass transfer coefficient of A in the jth species other than A (see equation 39)	m/s
L	mass flow rate of liquid	$kg/(s\cdot m^2)$
L_M	liquid flow rate	$kmol/(s\cdot m^2)$
$L^0{}_M$	generalized liquid flow rate, see equation 73	$kmol/(s\cdot m^2)$
L'_M	flow rate of solute-free solvent	$kmol/(s\cdot m^2)$
L'	liquid flow rate on a plate per width of stream	$m^3/(s\cdot m)$
l	bond length	m
l_0	equilibrium bond length	m
m	slope of equilibrium line	
N_A	flux of solute A through phase interface	$mol/(s\cdot m^2)$
N_G	number of gas-phase transfer units, see equation 52	
N_j	flux of component j through phase interface	$mol/(s\cdot m^2)$
N_l, N_s	length of linear hydrocarbon chains	
N_L	number of liquid-phase transfer units, see equation 55	
N_{OG}	number of overall gas-phase transfer units, see equation 58	
N_P	number of actual plates in the column	
N_T	N_{OG} for equimolar counterdiffusion, see equation 66	
N_{TP}	number of theoretical plates	
NTU_{ap}	N_{OG} calculated by equation 65, see also equation 82	
NTU	actual value of N_{OG} under the influence of axial dispersion, see equation 83	

Symbol	Definition	Units
P	pressure	Pa
p_A	partial pressure of A	Pa
p_{A_i}	partial pressure of A at the interface	Pa
P_s	vapor pressure of a pure component	Pa
Pe	uh/D_{ax}, dimensionless Peclet number	
Pe_i	Peclet number specifically defined for phase i, $i = x$ or y	
Pe_{HTU}	uH_{OG}/D_{ax}, dimensionless HTU Peclet number, see equation 84	
$Pe_{HTU,i}$	Peclet number specifically defined for phase i, $i = x$ or y, see equation 86	
R	L_M/G_M, *flow ratio*	
r	distance between interaction sites (atoms)	m
r_{ij}	relation velocity for species i in reaction j	kmol/m^{3}s
s	surface renewal rate, equation 41	s^{-1}
Sc	$\mu/\rho D$, the dimensionless Schmidt number	
T	temperature	°C or K
t_A	$\Sigma_j N_j/N_A$, parameter indicating the degree of counterdiffusion	
t_L	residence time of liquid on plate, see equation 104	s
U	total (intramolecular and intermolecular) interaction energy	J/kmol
U_A	linear velocity of diffusion of solute A	m/s
U_j	linear velocity of diffusion of the jth species other than the solute A	m/s
u	superficial velocity of gas or liquid phase	m/s
V^{LJ}	Lennard–Jones interaction potential	J/kmol
$V_{stretching}$	bond stretching potential	J/kmol
$V_{bending}$	bond bending potential	J/kmol
$V_{torsion}$	bond torsion potential	J/kmol
X_f	film factor, see equation 24	
X^0_A	$x_A/(1-t_A x_A)$, generalized liquid concentration, see equation 73	
X'_A	$x_A/(1-x_A)$, liquid mole ratio	
x_A	liquid mole fraction of solute	
x_j	mole fraction of the jth species other than A	
x_A	arithmetic mean of mole fraction of A over diffusion path	
x_j	arithmetic mean of x_j over diffusion path	
x_{Ab}	mole fraction in bulk of the liquid phase	
x_{Ai} or x_i	liquid mole fraction of solute at the phase interface	
x_{BM}	logarithmic mean of solvent concentration between the phase interface and the bulk of the liquid, see equation 18	
Y	moles absorbed component per mole of entering vapor, equation 98	
Y'	$y/(1-y)$, mole ratio	
Y^0_A	$Y_A/(1-t_A y_A)$, generalized gas concentration, see equation 64	
Y_f	film factor, see equation 23	
y^*_A	mx_A, concentration in equilibrium with bulk liquid	
y_{Ab}	mole fraction in bulk of gas phase	
y_{A_i} or y_i	gas mole fraction of solute at phase interface	
y_{BM}	logarithmic mean of inert gas concentration between the phase interface and the bulk of the gas phase, see equation 15	
y^*_{BM}	$[(1-y_A)(1-y^*_A)]/\ln[(1-y_A)/(1-y^*_A)]$, logarithmic mean of inert gas concentration between the equilibrium concentration and the bulk of the gas phase	

Symbol	Definition	Units
Y_f^*	$[(1-t_A y_A)-(1-t_A y_A^*)]/\ln[(1-t_A y_A)/(1-t_A y_A^*)]$, overall gas-phase film factor	
z_0	thickness of diffusion layer	m
z_L	length of liquid travel on tray	m
Δg_j	total amount of component j absorbed	kmol/(s·m^2)
$\Delta H_{Rij}\,(T)$	molar enthalpy of reaction	J/kmol
ΔT_{max}	temperature associated with internal temperature maximum °C or K	
δ	film thickness	m
ε_{ij}	Lennard–Iones first interaction constant (potential well depth parameter)	J/kmol
θ	bond angle	rad
θ_0	equilibrium bond angle	rad
μ	viscosity	mPa·s(=cP)
μ	chemical potential	J/kmol
ϕ	dihedral or torison angle	rad
Γ	Correction factor for thermodynamic nonidealities in diffusion equations, see equation 33	
ρ	density	mol/m^3
$\overline{\rho}$	mean density of liquid phase	mol/m^3, mol/L, or g/cm^3
σ	surface tension	N/m
σ_{ij}	Lennard–Jones second interaction constant (atom size parameter)	m
ϕ	packing parameter for equation 93	m
ψ	packing parameter for equation 94	m

SUBSCRIPTS

av	average
A	component A, solute
B	component B, usually nondiffusing
G	gas
L	liquid
b	in the bulk; this symbol is normally omitted
i	at gas–liquid interface
0	liquid feed for plate columns
x	pertaining to liquid phase
y	pertaining to gas phase
M	molar quantity
n	referring to stream leaving the nth tray
1	bottom of a packed column
2	top of a packed column

BIBLIOGRAPHY

"Absorption" in *ECT* 1st ed., Vol. 1, pp. 14–32, by E. G. Scheibel, Hoffmann-La Roche, Inc.; in *ECT* 2nd ed., Vol. 1, pp. 44–77, by F. A. Zenz, Squires International, Inc.; in *ECT* 3rd ed., Vol. 1, pp. 53–96, by C. W. Wilke and Urs von Stockar, University of California, Berkeley; in *ECT* 4th ed., Vol. 1, pp. 38–93, by Urs von Stockar, École Polytechnique Fédérale, Lausanne and C. W. Wilke, University of California, Berkeley; "Absorption" in *ECT* (online), posting date: December 4, 2000, by Urs von Stockar, École Polytechnique Fédérale, Lausanne and C. W. Wilke, University of Berkeley.

CITED PUBLICATIONS

1. F. A. Zenz, *Chem. Eng.* **120**, 1972 (Nov. 13, 1972).
2. R. E. Treybal, *Mass Transfer Operations*, 3rd ed., McGraw-Hill Book Co., Inc., New York, 1980.
3. W. S. Norman, Absorption, *Distillation and Cooling Towers*, Longmans, Green & Co., Ltd. (Wiley) New York, 1962.
4. T. K. Sherwood, R. L. Pigford, and C. R. Wilke, *Mass Transfer*, McGraw-Hill Book Co., Inc., New York, 1975.
5. A. Mersmann, H. Hofer, and J. Stichlmair, *Ger. Chem. Eng.* **2**, 249 (1979).
6. R. H. Perry, D. Green and J. O. Maloney, eds., *Perry's Chemical Engineer's Handbook*, 7th ed., McGraw-Hill Book Co., Inc., New York, 1997.
7. J. M. Prausnitz, R. N. Lichtenhaler, and E. Gomes de Azevedo, *Molecular Thermodynamics of Fluid-Phase Equilibria*, 3rd ed., Prentice-Hall, Englewood Cliffs, N. J., 1986.
8. R. C. Reid, J. M. Prausnitz, and B. E. Poling, *The Properties of Gases and Liquids*. 4th ed., McGraw-Hill Book Co., New York, 1988.
9. A. S. Kertes and co-workers, *Solubility Data Series*, Pergamon Press, Oxford, U.K., 1979.
10. W. C. Edmister, *Applied Hydrocarbon Thermodynamics*, Gulf Publishing Co., Houston, Tex., 1961.
11. N. B. Vargaftik, *Tables on the Thermophysical Properties of Liquids and Gases*, John Wiley & Sons, Inc., New York, 1975.
12. R. Battino, *Solubility Data Series*, Pergamon Press, Oxford, 1981.
13. J. Gmehling and U. Onken, *Vapor-Liquid Equilibrium Data Collection*. Chemistry Data Series, Dechema, Frankfurt, 1977 ff.
14. M. P. Allen and D. J. Tildesley, *Computer Simulation of Liquids*, Oxfort University Press, 1987.
15. D. Frenkel and B. Smit,*Understanding of Molecular Simulation From Algorithms to Applications*, Academic Press, 1999.
16. R. J. Sadus, *Molecular Simulation of Fluids: Theory, Algorithms and Object-Orientation*, Elsevier, New York, 1999.
17. W. J. Ward and J. A. Quinn, *AIChE J* **11**, 1005 (1965).
18. C. K. Brooks, III, M. Karplus, and B. M. Pettitt, Proteins: a Theoretical Perspective of Dynamics, Structure and Thermodynamics, in *Advances in Chemical Physics*, Vol. LXXI, John Wiley & Sons, Inc., New York, 1988.
19. P. Van der Ploeg and H. J. C. Berendsen, *J. Chem. Phys.* **76**, 3271 (1982).
20. J. P. Ryckaert and A. Bellemans, *Chem. Phys. Lett.* **30**, 123 (1975).
21. P. J. Flory, *Statistical Mechanics of Chain Molecules*, Interscience, New York, 1969.
22. A. R. Leach, *Molecular Modeling. Principles and Applications*, Longman, 1996.
23. W. B. Kay, *Ind. Eng. Chem.* **30**, 459 (1938).
24. F. Favari, A. Bertucco, N. Elvassore, and M. Fermeglia, *Chem. Eng. Sci.* **55**, 2379 (2000).
25. P. Paricaud, A. Galindo, and G. Jackson, *Fluid Phase Equil.* **194**, 87 (2002).
26. F. Tumakaka, J. Gross, and G. Sadowski, *Phase Equil.* **194**, 541 (2002).
27. M. Laso, J. J. de Pablo, and U. W. J. Suter, *Chem. Phys.* **97**, 2817 (1992).
28. N. F. A. van der Vegt, *J. Memb. Sci.* **205**, 125 (2002).
29. K. S. Shing, K. E. Gubbins, and K. Lucas, *Mol. Phys.* **65**, 1235 (1988).
30. M. Laso, J. J. De Pablo, and U. W. Suter, *J. Chem. Phys.* **97**(4), 2817 (1992).
31. S. Murad and S. Gupta, *Fluid Ph. Equil.* **187**, 29 (2001).
32. W. G. Whitman, *Chem. Metall. Eng.* **29**, 147 (1923).

33. A. F. Ward and L. H. Brooks, *Trans. Faraday Soc.* **48**, 1124 (1952).
34. E. J. Cullen and J. F. Davidson, *Trans. Faraday Soc.* **53**, 113 (1957).
35. J. L. Duda and J. S. Vrentas, *AIChE J* **14**, 286 (1968).
36. S. Lynn, J. R. Straatemeier, and H. Kramers, *Chem. Eng. Sci.* **4**, 58 (1955).
37. R. W. Schrage, *A Theoretical Study of Interface Mass Transfer*, Columbia University, New York, 1953.
38. B. Paul, *J. Am. Rocket Soc.* 1321 (Sept. 1962).
39. L. V. Delaney and L. C. Eagleton, *AIChE J* **8**, 418 (1962).
40. R. Cartier, D. Pindzola, and P. E. Bruins, *Ind. Eng. Chem.* **51**, 1409 (1959).
41. N. A. Clontz, R. T. Johnson, W. L. McCabe, and R. W. Rousseau, *Ind. Eng. Chem. Fundam.* **11**, 368 (1972).
42. J. T. Davies and E. K. Rideal, *Adv. Chem. Eng.* **4**, 1 (1963).
43. C. J. King, *AIChE J* **10**, 671 (1964).
44. R. B. Bird, W. E. Stewart, and E. N. Lightfoot, *Transport Phenomena*, John Wiley & Sons, Inc., New York, 1960.
45. C. R. Wilke, *Chem. Eng. Prog.* **46**, 95 (1950).
46. Curtiss and Hirschfelder, *J. Chem. Phys.* **17**, 552 (1949).
47. J. A. Wesselingh and R. Krishna, "Mass Transfer" in *Multicomponent Mixtures*, Delft University Press, Delft, The Netherlands, 2000.
48. R. Krishna and R. Taylor, *Multicomponent Mass Transfer*, John Wiley & Sons, Inc., New York, 1993.
49. R. E. Cunningham and R. J. J. Williams, *Diffusion in Gases and Porous Media*, Plenum Press, 1980.
50. E. L. Cussler, *Diffusion: Mass Transfer in Fluid Systems*, 2nd ed., Cambridge University Press, Cambridge, UK, 1997.
51. R. Zarzycki, A. Chacuk, *Absorption fundamentals & applications*, Pergamon Press, New York, 1993.
52. G. Ackermann, *Forschungsheft V.D.I.* **382**, 1 (1937).
53. W. K. Lewis and W. G. Whitman, *Ind. Eng. Chem.* **16**, 1215 (1924).
54. J. L. Bravo, J. A. Rocha and J. R. Fair, *Hydrocarbon Processing*. **1**, 91 (1985).
55. Y. Djebbar and R. M. Narbaitz, *Wat. Sci. Tech.* **38**, 295 (1998).
56. K. Onda, H. Takeuchi, and Y. Okumoto, *J. Chem. Eng. Jpn.* **1**, 56 (1968).
57. R. Higbie, *Trans. Am. Inst. Chem. Eng.* **31**, 365 (1935).
58. P. V. Danckwerts, *Ind. Eng. Chem.* **43**, 1460 (1951).
59. M. J. W. Frank, J. A. M. Kuipers, W. P. M. Van Swaaij, *Chem. Eng. Sci.* **55**, 3739 (2000).
60. H. L. Toor and J. M. Marchelo, *AIChEJ* **4**, 97 (1958).
61. H. López-Arjona, R. Lobo and T. Viveros-García, *Chem. Eng. Sci.* **55**, 6897 (2000).
62. M. Brinkmann, M. Schafer, H.-J. Warnecke, and J. Pruss, *Comp.Chem. Eng.* **22**, 515 (1998).
63. T. H. Chilton and A. P. Colburn, *Ind. Eng. Chem.* **26**, 1183 (1934).
64. G. F. Froment, in *Chemical Reaction Engineering* (Advances in Chemistry Series 109), American Chemical Society, Washington, D. C., (1972) p. 19.
65. P. V. Danckwerts, *Gas-Liquid Reactions*, McGraw-Hill Book Co., Inc., New York, 1970.
66. D. W. van Krevelen and P. J. Hoftijzer, *Rec. Trav. Chim.* **67**, 563 (1948).
67. K. F. Loughlin, M. A. Abul-Hamayel, and L. C. Thomas, *AIChE* **31**, 1614 (1985).
68. M. P. Pradhan, N. J. Suchak, P. R. Walse, and J. B. Joshi, *Chem. Eng. Sci.* **24**, 4569 (1997).
69. M. P. Pradhan, J. B. Joshi, *Chem. Eng. Sci.* **55**, 1269 (2000).
70. Ph. Leckner, R. O. Pearson and R. T. Wood, *Chem. Eng. Progr.* **78**, 65 (1982).
71. A. L. Kohl and R. B. Nielsen, *Gas Purification*, 5th ed., Gulf Professional Publishing, Houston, 1997.

72. A. M. Goldstein, E. C. Brown, F. J. Heinzelmann and G. R. Say, *Energy Prog.* **7**, 67 (1986).
73. B. E. Roberts and Alan E. Mather, *Chem. Eng. Comm.* **65**, 105 (1988).
74. T. T. Teng and A. E. Mather, *J. Chem. Eng. Data*, **35**, 410 (1990).
75. D. Zhang, H.-J. Ng, and R. Veldman, GPA 78th Annual Convention, March, 1999.
76. J. Carroll, J. Maddocks, and H.-J. Ng, GPA 78th Annual Convention, March, 1999.
77. R. Baur, R. Taylor and R. Krishna, *Chem. Eng. Sci.* **56**, 2085 (2001).
78. D. H. Miles and G. M. Wilson, Annual Report to the API for 1974, October, 1975.
79. H. L. Clever, S. A. Johnson, and M. E. Derrick, *J. Phys. Chem. Ref. Data*, **14**, 631 (1985).
80. M. Luckas, K. Lucas and H. Roth, *AIChEJ* **40**, 1892 (1994).
81. G. Sartori, W. Ho, D. Savage, G. Chludzinski, and S. Wiechert, *Sep. Purif. Meth.* **16**, 171 (1987).
82. G. Astarita, D. W. Savage and A. Bisio, *Gas Treating with Chemical Solvents*, John Wiley & Sons, New York, 1983.
83. P. M. M. Blauwhoff, G. F. Versteegand, and W. P. M. van Swaaij, *Chem. Eng. Sci.* **38**, 1411 (1983).
84. A. K. Saha, S. S. Bandyopadhyay, and A. K. Biswas, *J. Chem. Eng. Data* **38**, 78 (1993).
85. G. Astarita, *Mass Transfer with Chemical Reaction*, Elsevier, Amsterdam, the Netherlands, 1966.
86. A. P. Colburn, *Trans. Am. Inst. Chem. Eng.* **35**, 211 (1939).
87. J. H. Wiegand, *Trans. Am. Inst. Chem. Eng.* **36**, 679 (1940).
88. J. D. Raal and M. K. Khurana, *Can. J. Chem. Eng.* **51**, 162 (1973).
89. C. R. Wilke and U. v. Stockar, *Ind. Eng. Chem. Fundam.* **16**, 88 (1977).
90. J. Stichlmair, *Chem. Ind. Technol.* **44**, 411 (1972).
91. J. R. Bourne, U. v. Stockar, and G. C. Coggan, *Ind. Eng. Chem. Process Des. Dev.* **13**, 124 (1974).
92. C. R. Wilke and U. von Stockar, *Ind. Eng. Chem. Fundam.* **16** (2), 94 (1977).
93. I. A. Furzer, *Ind. Eng. Chem. Fundam.* **23**, 159 (1984).
94. N. Kolev and Kr. Semkov, *Chem. Eng. Prog.* **19**, 175 (1985).
95. N. Kolev and Kr. Semkov, *Vt Verfahrenstechnik* **17**, 474 (1983).
96. W. E. Dunn, T. Vermeulen, C. R. Wilke, and T. T. Word, Report UCRL 10394, University of California Radiation Laboratory as cited in Ref. 4, 1962.
97. W. E. Dunn, T. Vermeulen, C. R. Wilke, and T. T. Word, *Ind. Eng. Chem. Fundam.* **16**, 116 (1977).
98. E. T. Woodburn, *AIChE J* **20**, 1003 (1974).
99. M. Richter, *Chem. Tech.* **30**, 294 (1978).
100. U. von Stockar and P. F. Cevey, *Ind. Eng. Chem. Process Res. Dev.* **23**, 717 (1984).
101. A. K. Bi, B. Duczmal, and P. Machniewski, *Chem. Eng. Sci.*, **56**, 6233 (2001).
102. S. Moustiri, G. Hebrard, S. S. Thakre, and M. Roustan, *Chem. Eng. Sci.* **56**, 1041 (2001).
103. F. H. Yin, A. Afacan, K. Nandakumar, and K. T. Chuang, 50th Canadian Chemical Engineering Conference, Montreal, 2000.
104. B. J. Vinci, B. J. Watten, and M. B. Timmons, *Aquac. Eng.* **15**, 1 (1996).
105. R. A. Davis, *Chem. Eng. Edu.* **27**, 20 (1993).
106. T. Miyauchi and T. Vermeulen, *Ind. Eng. Chem. Fundam.* **2**, 113 (1963).
107. C. A. Sleicher, *AIChE J* **5**, 145 (1959).
108. S. Stemerding and F. J. Zuiderweg, *Chem. Eng. CE* 156 (May 1963).
109. J. C. Mecklenburgh and S. Hartland, *The Theory of Backmixing*, Wiley-Interscience, New York, Chapt. 10, 1975.
110. J. S. Watson and H. D. Cochran, *Ind. Eng. Chem. Process Res. Dev.* **10**, 83 (1971).

111. U. von Stockar and Xiao-Ping Lu, *Ind. Eng. Process Chem. Res. Dev.* **30**, 673 (1991).
112. U. von Stockar, ACHEMASIA, (International Meeting on Chemical Engineering & Biotechnology, Beijing, China), Dechema & Ciesc, (1989). p. 43.
113. T. K. Sherwood and F. A. L. Holloway, *Trans. Inst. Am. Chem. Eng.* **36**, 39 (1940).
114. F. F. Rixon, *Trans. Instn. Chem. Eng.* **26**, 119 (1948).
115. H. A. Koch, L. F. Stutzman, H. A. Blum, and L. E. Hutchings, *Chem. Eng. Prog.* **45**, 677 (1949).
116. E. L. Knoedler and C. F. Bonilla, *Chem. Eng. Prog.* **50**, 125 (1954).
117. J. E. Vivian and C. J. King, *AIChE J* **120**, 221 (1964).
118. D. Cornell, W. G. Knapp, and J. R. Fair, *Chem. Eng. Prog.* **56**, 68 (1960).
119. W. L. Bolles and J. R. Fair, *Chem. Eng.* **89**(July 12), 109 (1982).
120. P. H. Au-Yeung and A. B. Ponter, *Can. J. Chem. Eng.* **61**, 481 (1983).
121. D. M. Mohunta, A. S. Vaidyanathan, and G. S. Laddha, *Ind. Chem. Eng.* **11**, 73 (1969).
122. M. De Brito, U. von Stockar, A. Menéndez, P. Bomio and M. Laso, *Ind. Eng. Chem. Res.* **33**, 647 (1994).
123. R. Baur, A. P. Higler, R. Taylor, R. Krishna, *Chem. Eng. J.* **76**, 33 (2000).
124. M. de Brito, U. von Stockar, *IChE Symp. Ser.* **128**, B137 (1991).
125. J. B. Zech and A. B. Mersmann, *IChE Symp. Ser.* **56**, 39 (1979).
126. R. Mangers and A. B. Ponter, *Ind. Eng. Chem. Process Des. Dev.* **19**, 530 (1980).
127. M. S. Shi and A. B. Mersmann, *Ger. Chem. Eng.* **8**, 87 (1985).
128. R. Billet and M. Schultes, Paper given at AIChE Annual Meeting, Washington, D.C., 1988.
129. D. W. van Krevelen and P. J. Hoftijzer, *Rec. Trav. Chim. Pays-Bas* **66**, 49 (1947).
130. H. L. Schulman, C. F. Ulrich, A. Z. Proulx, and J. O. Zimmerman, *AIChE J* **1**, 253 (1955).
131. R. Billet, *Packed Column Analysis and Design*, Ruhr-Universität, Bochum (1989).
132. M. Laso, M. de Brito, P. Bomio, U. von Stockar, *Chem. Eng. J.* **58**, 251 (1995).
133. J. F. Davidson, *Trans. Inst. Chem. Eng.* **37**, 131 (1959).
134. J. Bridgewater and A. M. Scott, *Trans. Inst. Chem. Eng.* **52**, 317 (1974).
135. A. B. Ponter and P. H. Au-Yeung, *Can. J. Chem. Eng.* **60**, 94 (1982).
136. R. Echarte, H. Campana, and E. A. Brignole, *Ind. Eng. Chem. Process Des. Dev.* **23**, 349 (1984).
137. E. J. Lynch and C. R. Wilke, *AIChE J* **1**, 9 (1955).
138. H. L. Shulman, C. F. Ullrich, and N. Wells, *AIChE J* **1**, 247 (1955).
139. L. Spiegel and W. Meier, *Chem. Eng. Symp. Ser.* **104**, A203 (1987).
140. B. W. Gamson, G. Thodos, and O. A. Hougen, *Trans. Am. Inst. Chem. Eng.* **39**, 1 (1943).
141. R. G. Eckert and O. A. Hougen, *Chem. Eng. Prog.* **45**, 188 (1949).
142. C. R. Wilke and O. A. Hougen, *Trans. Am. Inst. Chem. Eng.* **41**, 445 (1945).
143. M. Hobson and G. Thodos, *Chem. Eng. Prog.* **47**, 370 (1951).
144. L. Fellinger, Ph.D., Dissertation, Massachusetts Institute of Technology, Boston, 1941 (see also Ref. 186).
145. J. L. Bravo and J. R. Fair, *Ind. Eng. Chem. Process Des. Dev.* **21**, 162 (1982).
146. L. Chunxi and W. Fürst, *Chem. Eng. Sci.* **55**, 2975 (2000).
147. F. Y. Jou, J. J. Carroll, A. E. Mather, and F. D. Otto, *Can. J. of Chem. Eng.* **71**, 264 (1993).
148. R. L. Kent and B. Eisenberg, *Hydrocarbon Proc.* **55**, 87 (1976).
149. G. Kuranov, B. Rumpf, G. Maurer, and N. A. Smirnova, *Fluid Phase Equilib.* **136**, 147 (1997).
150. M. L. Posey and G. T. Rochelle, *Ind. Chem. Eng. Res.* **36**, 3944 (1997).

151. E. B. Rinker, S. S. Ashour, and O. C. Sandall, *Chem. Eng. Sci.* **50**, 755 (1995).
152. D. P. Hagewiesche, S. S. Ashour, H. A. Al-Ghawas, and O. C. Sandall, *Chem. Eng. Sci.* **50**, 1071 (1995).
153. C. H. Liao and M. H. Li, *Chem. Eng. Sci.* **57**, 4569 (2002).
154. H. S. Fogler, *Elements of Chemical Reaction Engineering*, 3rd ed., Prentice Hall, 1998.
155. W. H. Press, A. Teukolsky, W. T. Vetterling, and B. P. Flannery, *Numerical Recipes in C++, The Art of Scientific Computing*, 2nd ed., Cambridge University Press, 2002.
156. T. K. Sherwood, G. H. Shipley, and F. A. L. Holloway, *Ind. Eng. Chem.* **30**, 765 (1938).
157. W. E. Lobo, L. Friend, F. Hashmall, and F. Zenz, *Trans. Am. Inst. Chem. Eng.* **41**, 693 (1945).
158. F. A. Zenz and R. A. Eckert, *Pet. Refiner.* **40**, 130 (1961).
159. R. A. Eckert, *Chem. Eng. Prog.* **66**, 39 (1970).
160. J. R. Fair, D. E. Steinmeyer, W. R. Penney, and B. B. Crocker, in Ref. 6, pp. 18–23.
161. E. V. Murphree, *Ind. Eng. Chem.* **17**, 474 (1925).
162. A. Kremser, *Nat. Pet. News* **22**(21), 42 (1930).
163. G. G. Brown and M. Souders, *Oil Gas J.* **31**(5), 34 (1932).
164. M. Souders and G. G. Brown, *Ind. Eng. Chem.* **24**, 519 (1932).
165. G. Horton and W. B. Franklin, *Ind. Eng. Chem.* **32**, 1384 (1940).
166. W. C. Edmister, *Ind. Eng. Chem.* **35**, 837 (1943).
167. G. G. Brown and M. Souders, *The Science of Petroleum*, Vol. 2, Oxford University Press, New York, Sect. 25, p. 1557 (1938).
168. J. R. Bourne, U. v. Stockar, and G. C. Coggan, *Ind. Eng. Chem. Process Des. Dev.* **13**, 115 (1974).
169. J. Stichlmair and A. Mersmann, *Chem. Ing. Technol.* **43**, 17 (1971).
170. U. von Stockar, *Gasabsorption mit Wärmeeffekten*, Diss. Nr 4917, ETH-Zurich (1973).
171. W. R. Owens and R. N. Maddox, *Ind. Eng. Chem.* **60**, 14 (1968).
172. H. G. Drickamer and J. R. Bradford, *Trans. Am. Inst. Chem. Eng.* **39**, 319 (1943).
173. A. E. O'Connell, *Trans. Am. Inst. Chem. Eng.* **42**, 741 (1946).
174. Research Committee, *Bubble Tray Design Manual*, American Institute of Chemical Engineers, New York, 1958.
175. W. K. Lewis, *Ind. Eng. Chem.* **28**, 399 (1936).
176. M. Nord, *Trans. Am. Inst. Chem. Eng.* **42**, 863 (1946).
177. M. F. Gautreaux and H. E. O'Connell, *Chem. Eng. Prog.* **51**, 232 (1955).
178. E. D. Oliver and C. C. Watson, *AIChE J* **2**, 18 (1956).
179. L. A. Warzel, Ph.D. Dissertation, University of Michigan, Ann Arbor, Mich., 1955.
180. V. M. Ramm, *Absorption of Gases*, Israel Program for Scientific Translations, Jerusalem, 1968 Chapt. 3.
181. G. G. Brown, M. Souders, H. V. Nyland, and W. H. Hessler, *Ind. Eng. Chem.* **27**, 383 (1935).
182. A. P. Colburn, *Ind. Eng. Chem.* **28**, 526 (1936).
183. C. P. Strand, *Chem. Eng. Prog.* **59**, 58 (1963).
184. M. Souders and G. G. Brown, *Ind. Eng. Chem.* **26**, 98 (1934).
185. J. R. Fair, *Petro/Chem Eng.* **33**(10), 45 (Sept. 1961).
186. T. K. Sherwood and R. L. Pigford, *Absorption and Extraction*, McGraw-Hill Book Co. Inc., New York, 1952.

GENERAL REFERENCES

References 2–4, 6–8, 21, 22, 37, 44, 47, 48, 50, 58, 65, 85, 109, and 154 are general references.
A. H. P. Skelland, *Diffusional Mass Transfer*, John Wiley & Sons, Inc., New York, 1974.

MANUEL LASO
Universidad Politécnica de Madrid, ETSII (Spain)
URS VON STOCKAR
École Polytechnique Fédérale de Lausanne